Trend detection and seasonal variation of tropospheric NO_2 over China.

中国 上空二氧化氮 浓度变化趋势 监测

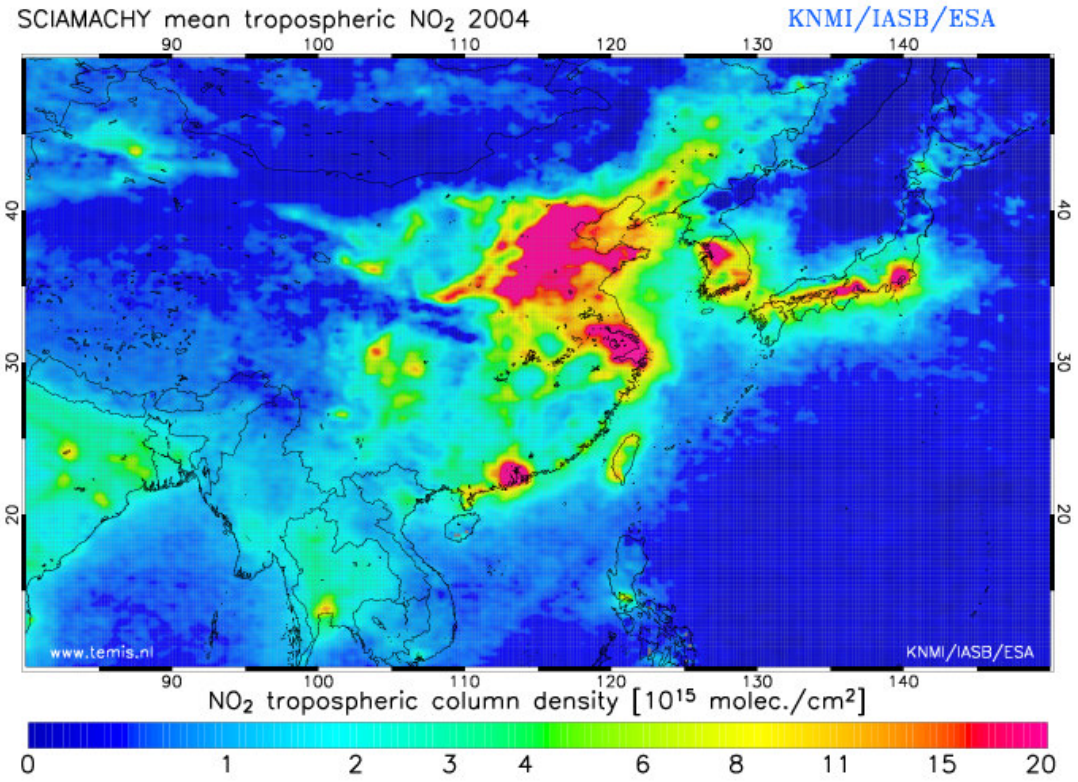

D.H.M.U. Peters
June 2005

Supervisors: dr. R.J. van der A (KNMI, De Bilt)
prof. dr. H. Kelder (Eindhoven University of Technology; KNMI, De Bilt)

Eindhoven University of Technology
Department of Applied Physics

Index

Preface

The growing economy of China and air pollution are both important global issues. Recently the new air quality rules from the European Union make air pollution an important economical and political topic in the Netherlands. China on the other hand is frequently in the media due to the rapid development of the country and its accompanying opportunities.

This report brings air pollution and the economical development in China together. It focus on one of the consequences of the rapid growth of the economy in China; increasing emissions of pollutants. A closer look will be given on NO_2, which is one of the constituents of air pollution. The satellite instruments GOME and SCIAMACHY provide a dataset of almost ten years of atmospheric information. This dataset is used to perform a trend study on the tropospheric NO_2 columns over China.

The study is part of the "Air quality Monitoring and Forecasting In China" (AMFIC) project in the framework of the DRAGON programme. The DRAGON programme is the umbrella project for joint Sino and European studies and is initiated by the European Space Agency (ESA) and the Ministry of Science and Technology of China (MOST). The AMFIC project is a cooperation between the Royal Dutch Meteorological Institute (KNMI), TNO-FEL, Belgian Institute for Space Aeronomy (BIRA-IASB), Flemish Institute for Technological Research (VITO), University of Bremen and the National Satellite Meteorological Centre of China (NSMC).

In this report the results are presented of a one-year study carried out at the KNMI, of which one month was spend at the NSMC in Beijing. The work presented in this report tries to answer the next questions for China:

1. What is the trend in tropospheric NO_2 and what is the significance of this trend in the available nine years long dataset?
2. What is the seasonal variation of tropospheric NO_2?
3. How can we interpret the trend and the seasonal variation in tropospheric NO_2?

The first part of this report contains chapters with background information of the satellite instruments and NO_2 chemistry. Questions like; "What is the role of NO_2 in the troposphere?" and "How is NO_2 measured?" are answered. The last chapter of the first part focuses on present-day China to give the reader an impression of the recent economical developments in China.

The second part of report is based on a paper, which will be submitted to the *Journal of Geophysical Research*. It shows the input, methods and answers on the main questions of this report. In the appendices extra derivations and figures are shown. They were not shown in the article, but they complete the overview of the study.

1 Introduction to NO_x

Nitrogen oxides play an important role in chemistry of the atmosphere. They are one of the primary air pollution constituents. The two most important nitrogen oxides for the troposphere are nitric oxide (NO) and nitrogen dioxide (NO_2), often called "active nitrogen" and grouped together as NO_x. The focus of this research is the nitrogen dioxide concentration measured by the satellite instruments GOME and SCIAMACHY. However, the chemistry of nitric oxide and nitrogen dioxide cannot be separated.

NO_x is important for the ozone (O_3) and hydroxyl (OH) distribution in the atmosphere. The role of NO_x in the troposphere differs from the role of NO_x in the stratosphere. In the troposphere NO_x contributes to ozone production, while in the stratosphere NO_x play a role in ozone destruction. Because of the differences between tropospheric and stratospheric chemistry and the focus of this research is tropospheric NO_2, only the chemistry of tropospheric nitrogen oxides will be discussed. The NO_x concentration also influences the hydroxyl radical (OH) concentration. The hydroxyl radical is the primary oxidant in the troposphere. It is responsible for converting primary emissions to secondary products that can be removed from the atmosphere by wet and dry deposition. Because of this mechanism the OH radical is called the "atmospheric detergent".

In this chapter an overview of the chemistry of tropospheric nitrogen oxides is presented. First the health and environmental impact of NO_x will be shortly considered. Then in paragraph 1.2 the major sources and sinks of NO_x emission are presented. In the last part of this chapter the NO_x chemistry in the troposphere is treated. An overview of the most important NO_x reactions is given.

1.1 NO_x as pollutant

Short and long exposure to NO_x can induce health effects, especially in combination with other pollutants. Exposure to NO_x can lead to pulmonary damage and long-term exposure has been associated with respiratory symptoms. The combination of NO_2 and O_3 can exacerbate allergic reactions.

The emission of NO_x in combination with hydrocarbons can lead to smog production in summer months. High smog concentrations pose threats to animal, plant and human life. One of the hazardous components of smog is ozone (O_3). NO_x in combination with hydrocarbonates largely determine the ozone concentration in the boundary layer. Health effects caused by the exposure to smog are irritation of nose and throat, coughing, painful breathing and reduced lung function. Long-term exposure to smog can affect lung elasticity and the immune system. Recent studies also show a possible influence of smog on cardio-vascular diseases. In the position paper on nitrogen dioxide from the European Commission [1997] a threshold of 200 $\mu g/m^3$ is suggested, according to a Swedish study [Bylin, 1993] this value is the lowest effect level for asthmatics.

Environmental impacts of NO_x are mainly due to NO_x deposition and its role in ozone formation. Ozone can be transported and influences human life and damages vegetation far from the source. The major removal reaction of NO_x out of the atmosphere leads to HNO_3, which is together with H_2SO_4 the main component of acid precipitation. The deposition of

NO_x related particles lead to increase nitrogen loading in water bodies. This leads to an over stimulated growth of algae. This deterioration of the water quality is also known as eutrophication.

1.2 NO_x sources and sinks

Because NO_x is a key ingredient in the chemistry of the atmosphere it is important to know the major sources of NO_x. The sources can be distinguished in anthropogenic sources and natural sources. Olivier et al. [1998] investigated the global emissions for NO_x in 1990 [Table 1.1]. Table 1.1 shows that 75% of the total global emissions are from anthropogenic sources. Most of the anthropogenic NO_x emission occurs during combustion processes. Especially on the Northern Hemisphere the fossil fuel combustion supplies the majority of the NO_x emissions. Olivier et al. [1998] found that 70% of the global anthropogenic NO_x emissions are from fossil fuel combustion. The major fuel combustion sources are road transport, power plants, and industrial processes, contributing 31%, 20% and 5%, respectively to the total anthropogenic NO_x emission. Biomass burning is the other import anthropogenic source, with a contribution of 25% to the total anthropogenic NO_x emissions.

Major natural sources of NO_x are soil emissions and lightning, the estimated contribution is 50% and 35% respectively of the total global natural emissions. The soil NO_x emission is associated with the biological nitrogen cycle and follows from denitrifaction, nitrification processes.

Table 1.1. Global sources of atmospheric NO_x in 1990 and their uncertainty ranges in TG [N] $year^{-1}$, adopted from Olivier et al. [1998]. *The lighting source is adopted from Boersma et al. [2005]. ** Uncertainty range is included in the surface fossil fuel combustions.

Source	Emission	Uncertainty range
Total anthropogenic sources	**31.1**	**16-46**
- Fossil fuel combustion (surface)	21.3	13-31
- Biomass burning	7.7	3-15
- Aircraft**	0.6	-
- Industrial processes**	1.5	-
Total natural sources	**11.1**	**6-35**
- Soil microbial production	5.5	4-12
- Lightning*	4.0	2-20
- Atmospheric NH_3 oxidation to NO_x	0.9	0-1.6
- Stratospheric destruction of N_2O	0.7	0.4-1
Total antr. + Natural	**42.2**	**22-81**

Physical processes such as wet and dry deposition and incorporation in particles remove NO_x from the atmosphere. The most important removal reaction of NO_x is the formation of HNO_3,

$$NO_2 + OH \rightarrow HNO_3, \tag{1.1}$$

followed by the wet deposition of HNO_3, which leads to acidification. This removal mechanism only occurs during daytime, especially in summer, because OH is produced by light and the lifetime is very short. An other important removal reaction cycle is the formation of N_2O_5,

$$\begin{aligned} &NO_2 + O_3 \rightarrow NO_3 + O_2 \\ &NO_2 + NO_3 \rightarrow N_2O_5 \\ &N_2O_5 + H_2O / aerosol \rightarrow 2HNO_3 \end{aligned} \quad . \tag{1.2 a t/m c}$$

This removal cycle is dominating during night time and wintertime.

The major sources and sinks of NO_x are shown, also the effects of NO_x on human life are considered. The next paragraph will deal with the NO_x chemistry in the troposphere.

1.3 NO_x chemistry

Introduction

A fundamental concept of the NO_x chemistry in the atmosphere is the photo stationary state. After introduction of the photo stationary state the different regimes of NO_x concentration will be considered. Because NO_x species have a large influence in atmospheric chemistry, the reported lifetime of NO_x in different studies will be mentioned. At the end of this chapter a small overview of the NO_x chemistry is given.

As mentioned before nitrogen oxides have a large influence on the ozone concentration. To form ozone it is necessary to have a production of the O atom. In the stratosphere the O atom is produced by the photolysis of O_2. In the troposphere this reaction is negligible, because wavelengths responsible for this reaction are almost completely absorbed in the stratosphere. The major source of O atoms in the troposphere is the photolysis of NO_2,

$$NO_2 + h\upsilon \rightarrow NO + O. \tag{1.3}$$

This formation of the O atoms is immediately followed by the next reaction,

$$O + O_2 + M \rightarrow O_3 + M. \tag{1.4}$$

The molecule M represents any other molecule, especially N_2 or O_2, which absorbs the energy of the reaction. Reaction 1.4 is very fast due to the high concentration of O_2 and N_2 in the atmosphere. In reaction 1.5, the nitric oxide molecule is oxidized by ozone. This reaction completes the cycle with respect to nitrogen oxides and ozone,

$$NO + O_3 \rightarrow NO_2 + O_2. \tag{1.5}$$

In equilibrium these reactions are said to be in the photo stationary state and the concentrations of NO, NO_2 and O_3 are then given by

$$\frac{[NO_2]}{[NO]} = \frac{k_5[O_3]}{j_3}, \tag{1.6}$$

where k_5 is the rate of reaction for reaction 1.5 in (concentration)$^{-1}$ (time)$^{-1}$ and j_3 is the photo dissociation frequency for reaction 1.3 in (time)$^{-1}$. The photo stationary state does not lead to a net production of ozone.

For ozone production an alternative pathway is needed for NO_2 production, instead of reaction 1.5 that does consume ozone. This is provided by the reaction between NO and peroxy radicals (RO_2 and HO_2, with R a hydrocarbon with an H-atom subtracted). These peroxy radicals are formed by reaction of OH with CH_4, CO and non-methane hydrocarbons also known as volatile organic components (VOC's). The source of VOC's in the atmosphere is a range of human activities, including combustion and chemical manufacturing. This net ozone production is solar driven and initialized by OH. The reactions are catalytic with respect to NO_x and OH. Reaction cycle 1.8 is an example of a net ozone formation by consuming VOC's (RH). In Brasseur [1999] examples of other reaction cycles can be found.

$$\begin{aligned}
&OH + RH \rightarrow R + H_2O \\
&R + O_2 + M \rightarrow RO_2 + M \\
&RO_2 + NO \rightarrow RO + NO_2 \\
&RO + O_2 \rightarrow HO_2 + R'CHO \\
&HO_2 + NO \rightarrow OH + NO_2 \\
&2(NO_2 + h\upsilon \rightarrow NO + O) \\
&\underline{2(O + O_2 + M \rightarrow O_3 + M)} \\
&RH + 4O_2 + 2h\upsilon \rightarrow R'CHO + H_2O + 2O_3
\end{aligned} \tag{1.8 a t/m f}$$

The efficiency of ozone production depends on the NO_x concentration and the peroxy radical concentration. The ozone production is efficient in the low NO_x case and inefficient in the high NO_x concentration case. In very high NO_x cases the ozone concentration will even decrease again and in the upper NO_x limit no ozone is left, as is shown Figure 1.1.

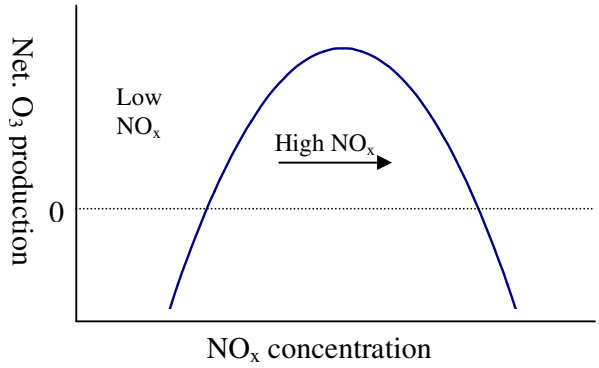

Figure 1.1. Schematic relation between the NO_x concentration and the net ozone production, for a fixed peroxy radical concentration, see Jacob [1999].

The definition of the low and high NO_x case is based on the influence of NO_x and peroxy radicals on the production of ozone [Kleinman, 1994]. In the low NO_x case, the NO_x concentration limits the ozone production, because there are enough peroxy radicals to react with NO. In the high NO_x case the peroxy radicals together with the NO_x concentration limit the ozone production. The critical concentration where the transition between the regimes takes place depends on the temperature and the concentration of other species.

The production of ozone occurs during daytime due to sunlight, see reaction 1.1. Therefore the daytime NO_x chemistry differs from the nighttime NO_x chemistry. During nighttime NO is converted in NO_2 by reaction 1.5, followed by the reaction cycle 1.2, therefore ozone is consumed during night time.

The low NO_x case

When the NO_x concentration is low the peroxy radicals are primarily formed by the oxidization of carbon monoxide (CO) and methane (CH_4), because other VOC's emissions are mainly in combination with high NO_x emissions. The formed peroxy radicals (HO_2 and CH_3O_2) can oxidize NO to NO_2 without consuming O_3. After the formation of NO_2, ozone is produced by reaction 1.3 and 1.4. In the low NO_x case the ozone production is linear dependent on the NO_x concentration, because there are sufficient peroxy radicals to react with NO and form O_3, therefore the ozone production is limited by the amount of NO_x.

The high NO_x case

In the high NO_x case the production of ozone is inefficient and depends on both the NO_x concentration and the amount of VOC's. High NO_x cases occur in regions with high anthropogenic and natural emissions. In these regions a large amount and variety of VOC's are available for oxidation processes to form peroxy radicals, following reaction 1.8a and 1.8b.

The higher amount of VOC's leads to more peroxy radicals, which in combination with more NO_x lead to a higher ozone production rate. Due to the high NO_x concentration the peroxy radicals will predominantly react with NO to form NO_2 followed by ozone production. If the NO_2 concentration is high enough, NO_2 will react with OH and reduce the efficiency of ozone production, because there is less OH available to initiate the consumption of VOC's to form ozone. In this case, the ozone production depends inversely with the NO_x concentration.

In urban areas, the NO_x concentrations can be much higher than the concentration of peroxy radicals. Then, the ozone production is limited by the peroxy radical concentration and in this situation O_3 can even be removed by reaction 1.5, which is the VOC's limited region of the ozone production. In Table 1.2 an overview of the different NO_x regimes and their influence on the ozone concentration is given.

Table 1.2. Overview of NO_x regimes and the corresponding leading reactions for ozone formation in the troposphere.

	Low NO_x	**Main reaction;** $HO_2+NO\rightarrow OH+NO_2$	**Limited:** NO_x
Photo stationary state $NO_2+h\upsilon\rightarrow NO+O$ $O+O_2+M\rightarrow O_3+M$ $NO+O_3\rightarrow NO_2+O_2$			
	High NO_x	**Main reaction:** $HO_2+NO\rightarrow OH+NO_2$ $RO_2+NO\rightarrow RO+NO_2$	**Limited:** NO_x VOC'S
			Limited: VOC'S

Lifetime of NO_2

The lifetime of NO_2 in the troposphere is of the order of one day and is altitude and seasonal dependent. It varies from hours in the continental boundary layer to 10 days in the upper troposphere. Because of this relative short lifetime the influence of transportation processes of NO_2 are rather small. The average lifetime is influenced by many factors like meteorological conditions, photolysis length and OH concentrations. The average NO_2 lifetime can be calculated in different ways. For instance, S. Beierle et al. [2003] used the weekly cycle of

NO_2 column above Germany, measured by GOME. They report a tropospheric NO_2 lifetime of 6 hours during summer and 18-24 hours during winters Leue et al. [2001] used the decay curve of the annual mean NO_2 column on the off-wind side of the East coast of the United States. They assumed an average wind and a first order decay. They found a NO_2 lifetime of 27 ± 3 hours.

The combination of the variability of the chemistry and emissions leads to a seasonal depended NO_2 concentration. The chemistry leads to a longer lifetime in the winter due to lower OH concentration in wintertime. This in combination with the winter maximum of anthropogenic emissions gives an expected maximum of NO_2 in wintertime. In wintertime, the anthropogenic emissions are usually higher due to heating of the buildings.

2 NO_2 measurements

The objective of the study is to perform a trend analysis on the tropospheric NO_2 column over China. In this chapter the input data of this study will be discussed. First, the instruments that measure the NO_2 column are introduced. Secondly, the retrieval of the tropospheric NO_2 column from the measurement will be explained.

2.1 The instruments

The input data for this research is measured by the satellite instruments GOME (Global Ozone Monitoring Experiment) and SCIAMACHY (SCanning Imaging Absorption SpectroMeter for Atmospheric CartograpHY). Main advantage of satellites is their capability of providing a full global mapping of the atmospheric composition. The ERS 2 platform with GOME aboard and the ENVISAT platform with SCIAMACHY aboard are both in a sun synchronise polar orbit. They fly 800 km above the earth surface and need 100 minutes for one orbit. Characteristic for GOME and SCIAMACHY is that they measure the light spectrum scattered back from the earth surface through the atmosphere. Molecules in the atmosphere have a wavelength dependent absorption. The amount of absorption, which is determined by comparing the reflection spectrum with a reference spectrum, is used to calculate the species concentration. The spectral information of NO_2 is found in the wavelength range of 425 nm to 450 nm.

The ERS 2 platform with GOME is launched in April 1995 and has provided useful NO_2 data from March 1996. The platform is crossing the Equator at 10:30 local time. Since June 2003 large parts of the world are not monitored due to a technical malfunction. The ground pixels measured by GOME are 320 km by 40 km, where the short side of the pixel is along the track, see Figure 2.1 for an example of a GOME track. In one scan from east to west GOME measures three pixels. A global coverage is achieved every three days. Except NO_2, GOME is able to detect the gases O_3, SO_2, BrO, H_2CO, H_2O and Aerosols.

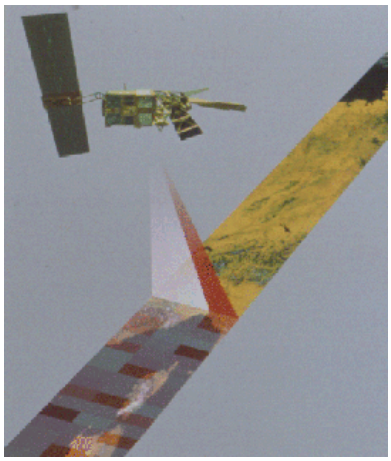

Figure 2.1. Example of a GOME track.

SCIAMACHY on board of the ENVISAT platform is launched in 2002 with a local Equator overpass time of 10:00. NO_2 data is available from January 2003. The ground pixel measured by SCIAMACHY is 60 km by 30 km, where the short side of the pixel is along the track. In one scan from east to west 16 pixels are measured. GOME had only the possibility to “look down”, also known as nadir view, SCIAMACHY has except the nadir view also the possibility to “look forward” trough the atmosphere, also known as limb view. In Figure 2.2 the concepts of nadir and limb view are illustrated. Because SCIAMACHY alternates between nadir view and limb view a global surface coverage is achieved every six days. In Figure 2.3 an example is given of the SCIAMACHY orbits and pixels for one day. At the open spaces

along a track the limb mode measurements take place, which are not shown. Only the SCIAMACHY nadir measurements are used in this study. SCIAMACHY measures, except NO_2, also O_3, SO_2, BrO, H_2CO, H_2O, CO, CO_2, CH_4, N_2O and Aerosols.

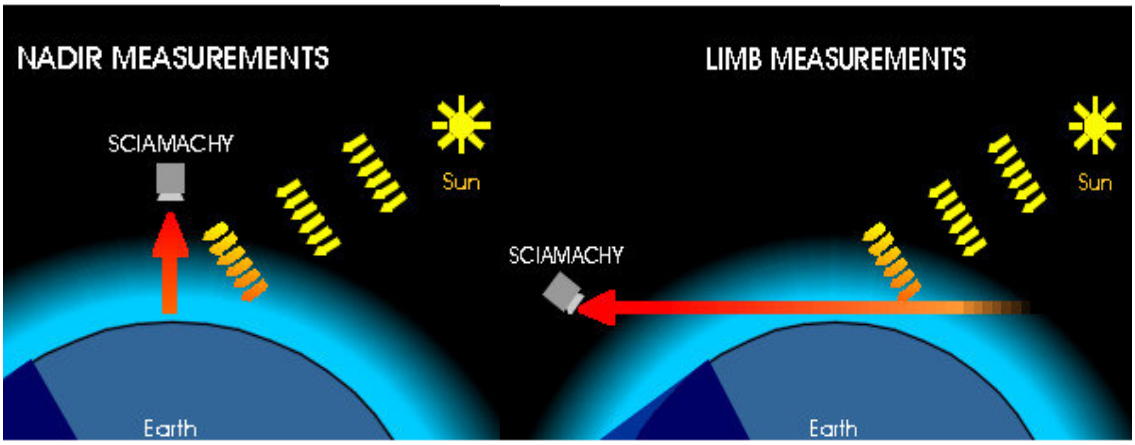

Figure 2.2. Illustration of the nadir viewing mode (left) and the limb viewing mode (right).

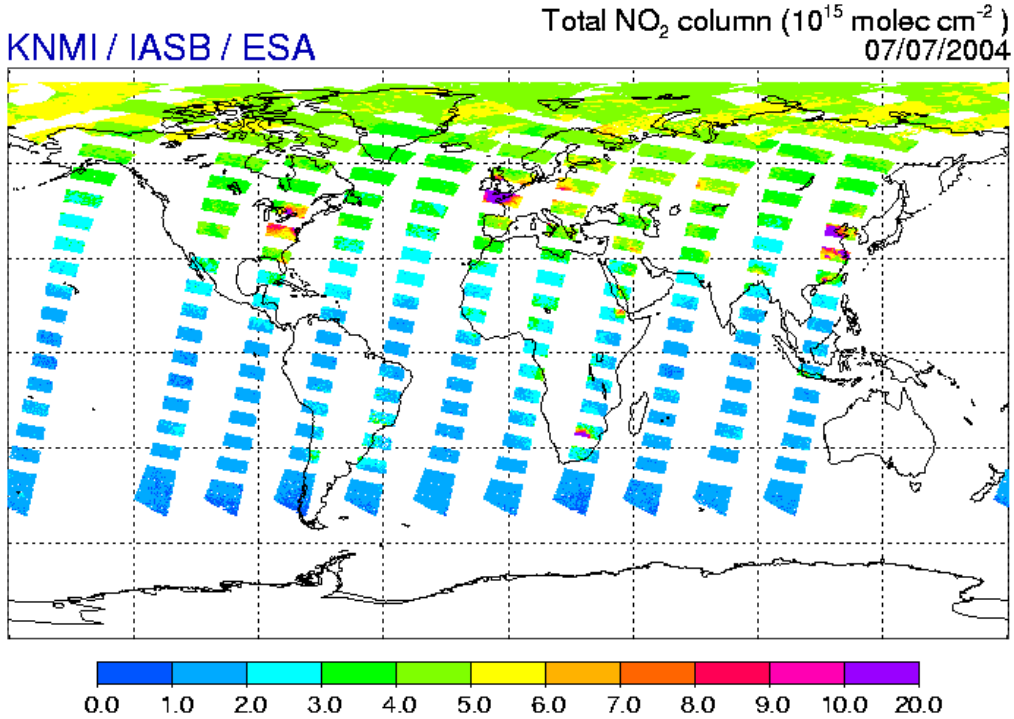

Figure 2.3. An example of the Nadir measurements of SCIAMACHY on 7th of July 2004. The open spaces along a track are due to Limb measurements.

2.2 Tropospheric NO_2 retrieval

The troposphere is the lowest domain of the atmosphere. It extends from the earth surface up to 8 – 18 km, depending on latitude and season. The stratosphere is the domain above the troposphere, it extends from the tropopause, the top of the troposphere and characterized by temperature inversion, to the stratopause, which is around 50 km high. Although the

atmosphere contains more domains, the troposphere and the stratosphere contain 99.9% of the total atmospheric mass.
In this study we are interested in the vertical tropospheric NO_2 concentration. A distinction is made between the troposphere and the stratosphere, because there are significant physical and chemical differences. The chemical differences with respect to NO_2 are already mentioned in chapter 1. The physical processes in the troposphere are characterized by vertical mixing, this in contrast with the transport in the stratosphere, which is dominated by horizontal mixing. The exchange between the stratosphere and the troposphere is relative small.

The vertical tropospheric NO_2 column (x_{tr}) can be obtained from the NO_2 total slant column (N_s), which is measured by the satellite instruments. In the next equation the relation between the vertical tropospheric column and the total slant column is given,

$$x_{tr} = \frac{N_s - N_{s,st}}{M_{tr}}, \tag{2.1}$$

where $N_{s,st}$ is the stratospheric slant column and M_{tr} is the tropospheric air mass factor. The terms in the equation will shortly be discussed, because each term affects the vertical tropospheric column.

GOME and SCIAMACHY measure an absorption spectrum. The total slant column density is retrieved from this spectrum by using the Differential Optical Absorption Spectroscopy technique (DOAS) [Platt, 1994]. The technique is based on the Beer – Lambert law, which describes the extinction of the solar radiation in an absorbing atmosphere. The total slant columns, used for this study, are processed at BIRA-IASB in Belgium. For more information on this process the reader is referred to Fayet and Van Roozendaal [2001].

The next step in the retrieval method is to determine the stratospheric slant column. Four methods can be distinguished from literature to calculate the stratospheric slant column.

1. Reference sector method [e.g. Martin et al., 2002]. NO_2 columns over remote areas are used to calculate a longitudinal constant stratospheric column.
2. A Chemical Transport Model (CTM) is used to calculate a stratospheric column [Richter et al., 2002].
3. The stratospheric column is determined from the SCIAMACHY limb view [Sierk et al., 2004].
4. Data assimilation [Eskes et al., 2003]. The column densities from a chemical transport model are made consistent with the satellite measurements. From this data assimilated product the stratospheric slant column density is derived.

The last technique is used for the calculation of the tropospheric NO_2 data in this study.

The last step is the calculation of the tropospheric air mass factor, which is the proportion between the vertical column density and the slant column density. The light path in the stratosphere is almost not affected by scattering. For this reason, the stratospheric air mass factor is approximately the same as the geometric air mass factor, which is determined by the position of the sun and the viewing angle of the satellite. In the troposphere the light path is strongly influenced by aerosols, albedo effects and scattering due to clouds. Therefore the tropospheric air mass factor is calculated with a radiative transfer model. The input

parameters to calculate the tropospheric air mass factor are cloud fraction, cloud height, surface albedo and solar geometry.

In Boersma et al. [2004] a quantitative error analysis for the tropospheric vertical NO_2 column is presented. For heavy polluted areas, the tropospheric NO_2 column is retrieved with a precision of 35% – 60%. The errors on the vertical tropospheric NO_2 are caused by the terms on the right hand side of equation 2.1 and show a dependence on the absolute value of the NO_2 column and has a minimum of approximately $1 \cdot 10^{15}$ molec/cm^2, this is shown in Figure 2.4. The minimum is caused by uncertainties in the total slant column and stratospheric slant column. For large tropospheric columns the error is dominated by uncertainties in the tropospheric air mass factor.

For more information on the tropospheric NO_2 product, the reader is referred to Eskes et al. [2003] and Boersma et al. [2004].

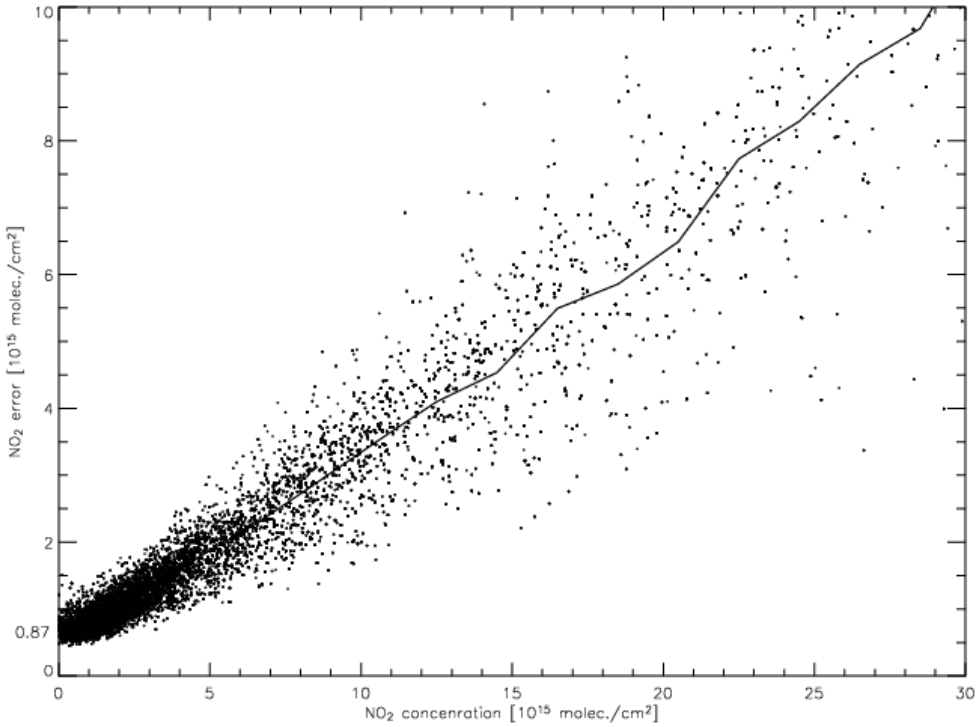

Figure 2.4. The relation between the measurement error and the absolute NO_2 column. The error is calculated as explained in Boersma et al. [2004]. The solid line shows the bin averages with bin width 2 10^{15} molec/cm^2. The value of the minimum error is also shown.

3 Recent economical developments in China

This chapter gives some more information on NO_x emissions in China, especially the expected changes. There is a large correlation between human activity and NO_x emissions. In table 1.1 it can be seen that 75% of the global NO_x sources are anthropogenic sources. In this chapter the growth and regional distribution of the human activity in China will be shown and can be used as an indication for the changes in NO_x emissions. Therefore, the figures in this chapter can be seen as background information of the human activities affecting the results presented in this report.

Economical development
Probably the best measure for the growth of anthropogenic activity is the growth of the Gross Domestic Product (GDP). Nowadays, China has one of the fastest growing economies of the world. In Figure 3.1 the growth of GDP is given for China during the last 15 years.

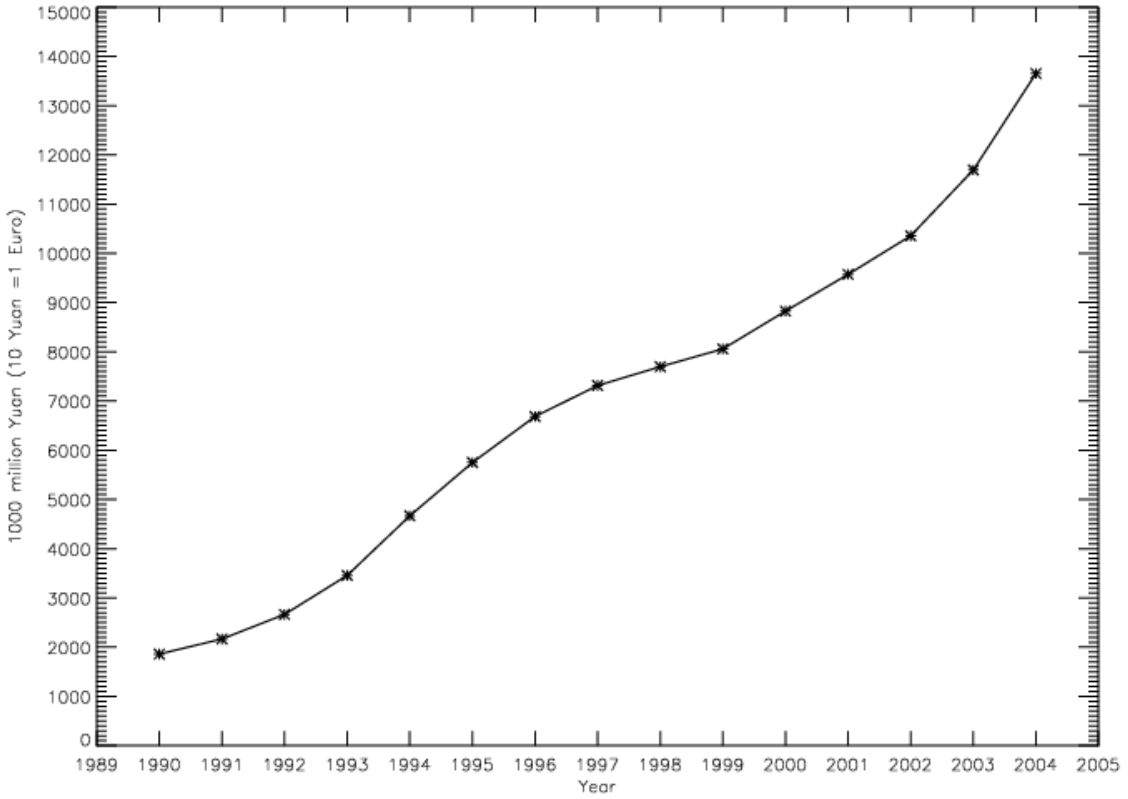

Figure 3.1. The growth of the Chinese Gross Domestic Product from 1990 to 2004. (Source: National Bureau of Statistics of China)

The figure shows that the Chinese economy is growing with a yearly average increase of about 9%. This economic growth goes together with an increase in industrial and human activity and leads to expected increasing emissions.
Streets et al. [2003] did an inventory of emissions in Asia for 2000. For China, they found that 39% of the anthropogenic NO_x emissions are caused by power generation followed by

industry and transportation both contributing about 25%. In the future Streets et al. [2003] expect increasing emissions due to a rapid growth in vehicle ownership. To get an indication of this rapid growth, the total number of vehicles in China is shown in Figure 3.2. for the years 1995 to 2002. The figure shows a doubling in the number of vehicles in six years and still the major part of the Chinese population does not have a car.

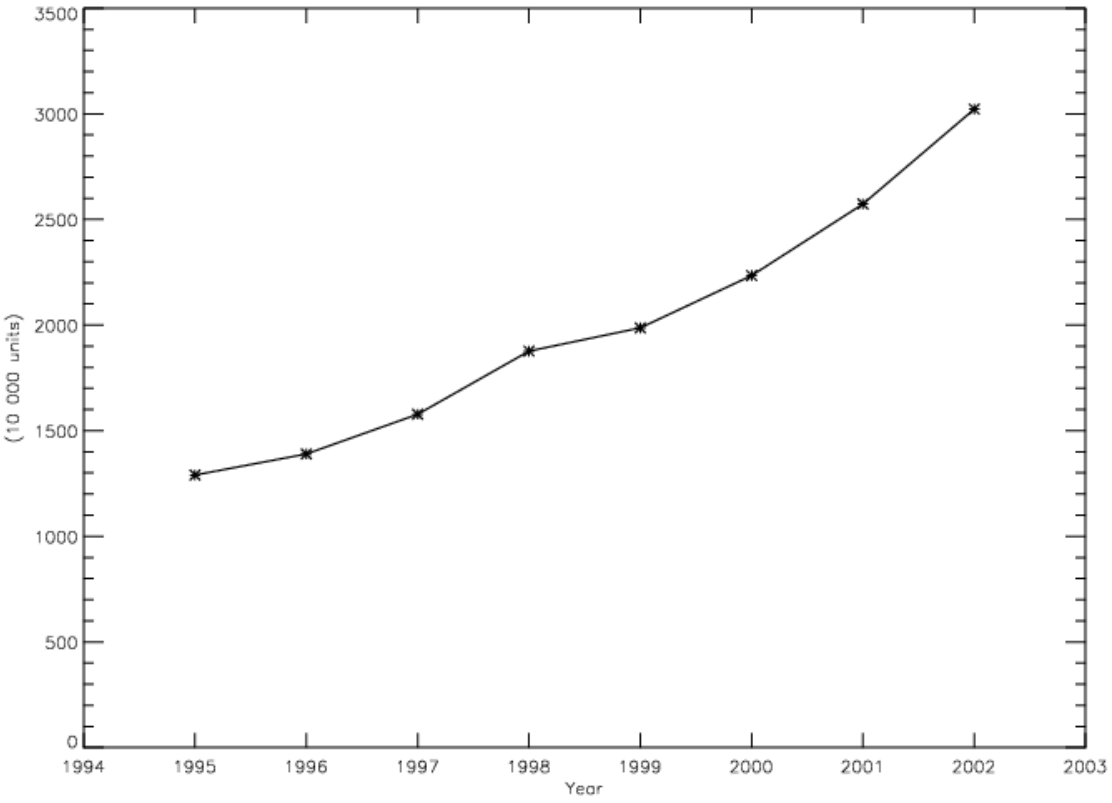

Figure 3.2. The number of vehicles (trucks and personal cars) in China from 1995 to 2002 (Source: National Bureau of Statistics of China)

Regional distribution in China

China is one of the largest countries of the world (230 times larger than the Netherlands) and therefore there are significant regional differences. The last part of the chapter shows the regional distribution of the population and energy consumption in China. The regional distribution of population and energy consumption implicates a comparable regional distribution of air pollution. Figure 3.3 clearly presents that the major part of the Chinese population is living in the eastern part of China. Therefore, it is expected that anthropogenic NO_x emissions will dominate in the East, especially in the major cities like Beijing, Shangai, Hong Kong and Xian.

To get a better impression of regional NO_x emissions, we use the regional distribution of power consumption. Because more than 90% of the Chinese power is generated by fossil fuel burning [NBS, 2004] and power generation is the most important contributor to NO_x emissions in China [Streets et al., 2003; Wang et al., 2004], it is expected that high energy consumption regions are the major contributors to anthropogenic emissions. Therefore

regional power consumption is used as an indication to make a distinction in NO_x emissions between the eastern provinces. In Figure 3.4 the regional power consumption is shown for the Chinese provinces during the period 1995-2002. To compare the values of different provinces the absolute consumption is scaled to the area of the provinces.
In Figure 3.4 it can be seen that the absolute power consumption is the largest in Shanghai.

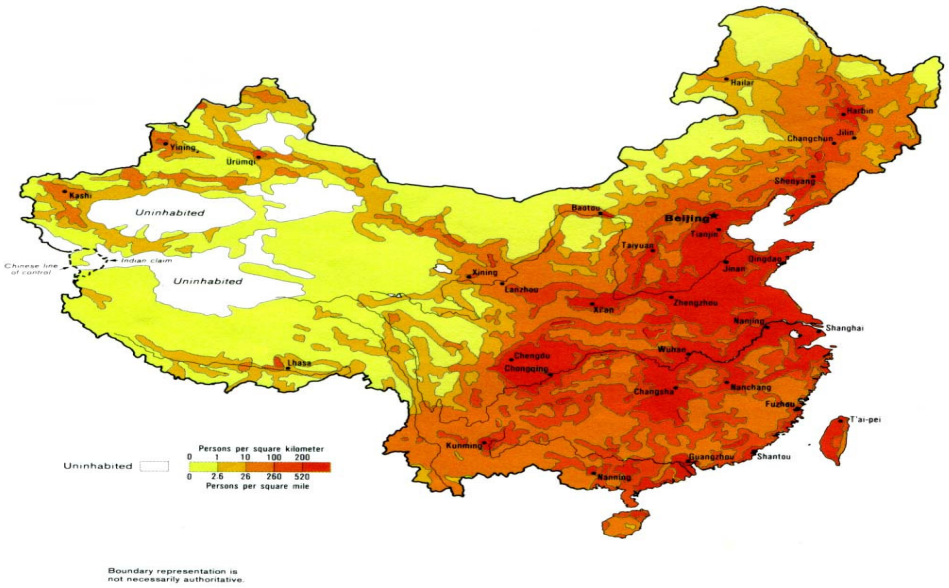

Figure 3.3. The population density in China. The red areas in East China are the major industrial and urbanized regions of China. (Source: map collection of University of Texas Libraries)

To get a feeling for these numbers we will compare them with the Dutch indications of human activity. The Dutch economy had an average growth of 2.7% during the years 1996-2004 [CBS]. During this period in the Netherlands, the number of vehicles increased with 30%. Although the yearly average NO_2 columns over the Netherlands and China are comparable nowadays, the increase of human activity in China is much larger. Based on this information a large increase of NO_x emissions is expected over China.

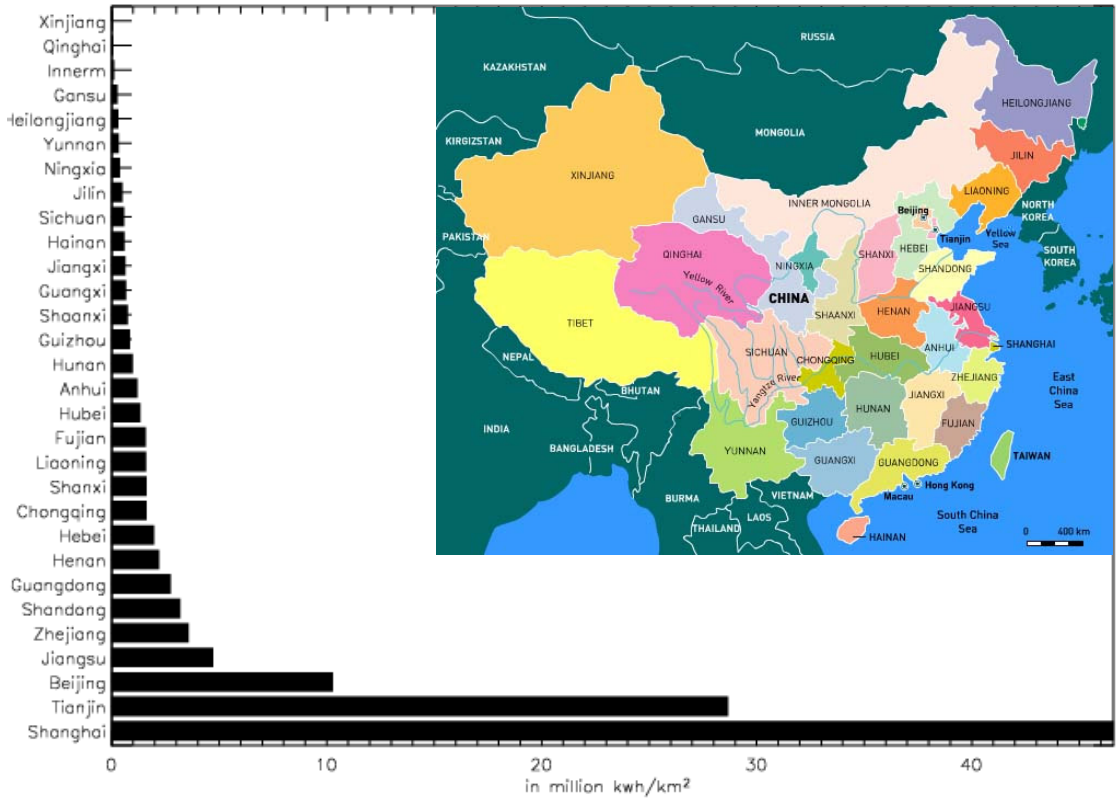

Figure 3.4. The regional distribution of the power consumption for each province during the period 1995-2002. The energy consumption is scaled to the area of the province. (Source: National Bureau of Statistics of China) The inset shows the map of China with the provinces.

4 Trend detection and seasonal variation in tropospheric NO_2 over China.

D.H.M.U. Peters[1,2], R.J. van der A[1], H. Eskes[1], K.F. Boersma[1], H.M. Kelder[1,2]
[1]Royal Netherlands Meteorological Institute, The Netherlands
[2] Eindhoven University of Technology, The Netherlands

Abstract
The results are presented of a trend study on the tropospheric NO_2 column over China, based on measurements from the satellite instruments GOME and SCIAMACHY. From these observations monthly averaged tropospheric NO_2 distributions are determined for the period 1996 to 2004 on a 1° by 1° grid. A linear model with a seasonal component is used to fit these time series. The variance and the autocorrelation of the noise are used to calculate the significance of the trend. The results show a large growth of tropospheric NO_2 over eastern China, especially above the industrial areas with a fast economical growth. For instance, Shanghai had a yearly increase in NO_2 columns of 25% in the period 1996-2004. The seasonal pattern of the NO_2 concentration shows a difference between East and West China. In the East a NO_2 maximum is found during wintertime, due to chemistry and anthropogenic activity. Contrary to this, in the western part of China the NO_2 concentration reach a maximum in summertime. This spatial difference correlates with the population distribution of China. Since there is negligible anthropogenic activity in West China this difference in seasonality of NO_2 is attributed to natural emissions in West China.

4.1 Introduction

Nitrogen oxides (NO_x=NO + NO_2) play an important role in atmospheric chemistry. NO_x has significant natural sources (e.g. lighting and soil emissions) and anthropogenic (e.g. biomass burning, fossil fuel combustion) sources. Global tropospheric NO_2 distributions are measured by the satellite instruments GOME (from 1995-2003) aboard ERS-2, SCIAMACHY (from 2002) aboard Envisat platform and OMI aboard EOS-AURA (from 2004). [Leue et al., 2001, Richter and Burrows, 2002; Martin et al., 2002; Boersma et al., 2004].
Recent studies on the tropospheric NO_2 columns show that the satellite measurements are suitable for improving emission inventories and air quality studies. Jaeglé et al. [2004] used GOME measurements over the Sahel to map the spatial and seasonal variations of NO_x, mainly caused by biomass burning and soil emissions. Martin et al. [2003] used GOME measurements to derive a top-down emission inventory. The top-down inventory in combination with bottom-up emission inventory is used to achieve an optimised posterior estimate of the global NO_x emissions. Boersma et al. [2005] used GOME measurements to estimate the global NO_x production from lightning by comparing modelled and measured spatial and temporal patterns of NO_2 in the tropics. In Blond et al. [2005] SCIAMACHY measurements are compared with an air quality model and ground measurements. They showed that SCIAMACHY measurements are able to monitor the air pollution over Europe and its day-to-day changes.
In this study we focus on China for the period 1996 to 2004. China has one of today's fastest growing economies of the world. This increase in economical activity is accompanied by a strong increase of emissions of tropospheric pollutants. We will combine GOME and

SCIAMACHY measurements to obtain a 9-year dataset that is suitable for a trend study. The strong increase in NO_x emissions in China is due to a increase in industry and traffic, see Wang et al. [2004]. These emissions are concentrated on the densely populated and industrialized Eastern part of China, as can be seen in Figure 4.1.

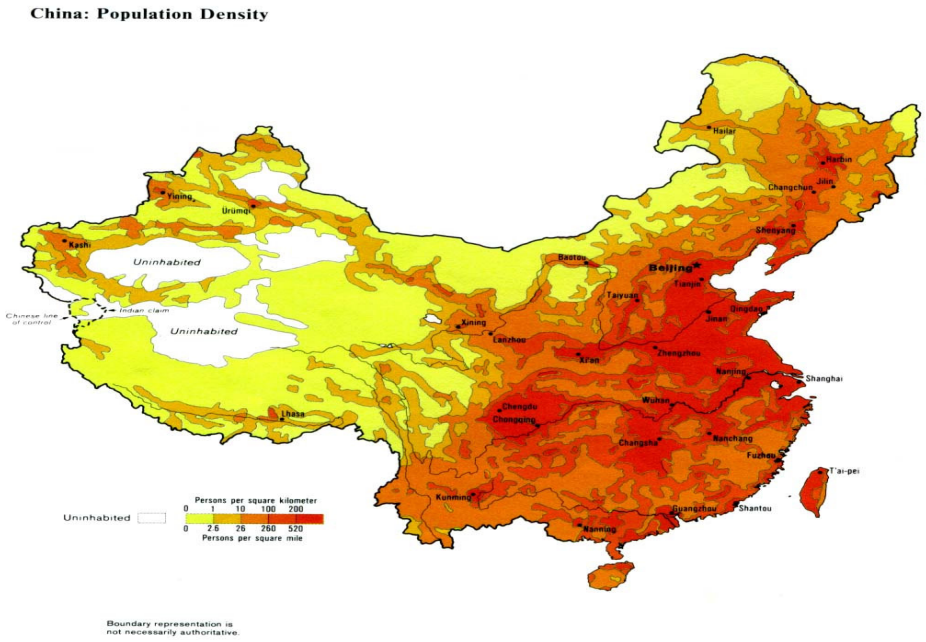

Figure 4.1. The population density in China. The red areas in East China are the major industrial and urbanized regions of China. (Courtesy of the University of Texas Libraries, The University of Texas at Austin.)

The combination of the variability in both chemistry and emissions leads to a seasonally dependent NO_2 concentration with an expected maximum of NO_2 in wintertime. The NO_2 lifetime is in the order of one day depending on many factors like meteorological conditions, photolysis time scale and OH concentrations. A higher actinic flux results in a higher OH concentration (if the water vapor concentration is high enough), which reacts with NO_2 to form HNO_3, the principal sink for NO_x. The emissions also show a variability. In wintertime, the anthropogenic emissions are usually higher due to heating of buildings. Beirle et al. [2003] found a variability with a weekly pattern in the NO_2 concentration above Europe, related to reduced anthropogenic emissions during the weekend. Above China no significant weekly cycle was observed.

The first objective of this study is to quantify the trend in tropospheric NO_2 using satellite data over China. Our second objective is to use the dataset to investigate the seasonality of the NO_2 columns over China. In section 4.2 a short introduction is given on tropospheric NO_2 retrieval method. The data analysis is described in section 4.3, which gives an overview of the applied model and statistics. The results of this study – the trend and the seasonal cycle of

tropospheric NO_2 over China – are shown in sections 4.4 and 4.5. Finally, in section 4.6 the conclusion and outlook of this study are presented.

4.2 Tropospheric NO_2 retrieval

The GOME and SCIAMACHY spectrometers measure backscattered light from the Earth in the UV and visible wavelength range. From the observed spectral features around 425-450 nm slant column densities (SCD) of NO_2 are derived with the Differential Optical Absorption Spectroscopy (DOAS) method [Platt, 1994]. The work presented here is based on slant columns retrieved from the satellite data by BIRA-IASB [Fayt and Van Roozendael, 2001]. The NO_2 stratospheric column is deduced from a chemistry-transport model assimilation run of the NO_2 slant column data. Subsequently, the assimilated stratospheric slant column is subtracted from the retrieved DOAS total slant column, resulting in a tropospheric slant column. The tropospheric NO2 columns are derived from these slant columns [Boersma et al., 2004]. Height-dependent air mass factor (AMF) lookup tables are based on calculations with the Doubling-Adding KNMI (DAK) radiative transfer model. The tropospheric vertical column is retrieved using TM4 [Dentener et al., 2003] tropospheric model profiles (co-located for each GOME and SCIAMACHY pixel individually) and combined with albedo and cloud information. The latter consists of cloud fraction and cloud top height derived by the FRESCO algorithm [Koelemeijer et al., 2003]. Only observations with an estimated cloud radiance fraction of less than 0.5 are used in this study. The retrieval includes surface albedo values constructed from a combination of the TOMS-Herman-Celarier-1997 and Koelemeijer-2003 surface reflectivity maps (available on a monthly basis). No aerosol correction is applied. This choice is based on the realization that the cloud retrieval will be influenced by aerosol as well, and is further motivated by the error analysis presented in the work of Boersma et al. [2004]. The final NO_2 column data product is publicly available on the TEMIS project website (http://www.temis.nl) with detailed error estimates and kernel information [Eskes and Boersma, 2003].

In Figure 4.2 the year average tropospheric NO_2 column of 2004 is given. The Figure shows high concentration above the highly populated regions like Beijing, Shanghai, Hong Kong and South Korea. It can also be seen that the satellite is detecting the emissions around the Yellow river (Huang He). Over western China, low NO_2 columns are observed except over the large city Urumqi in the Northwest.

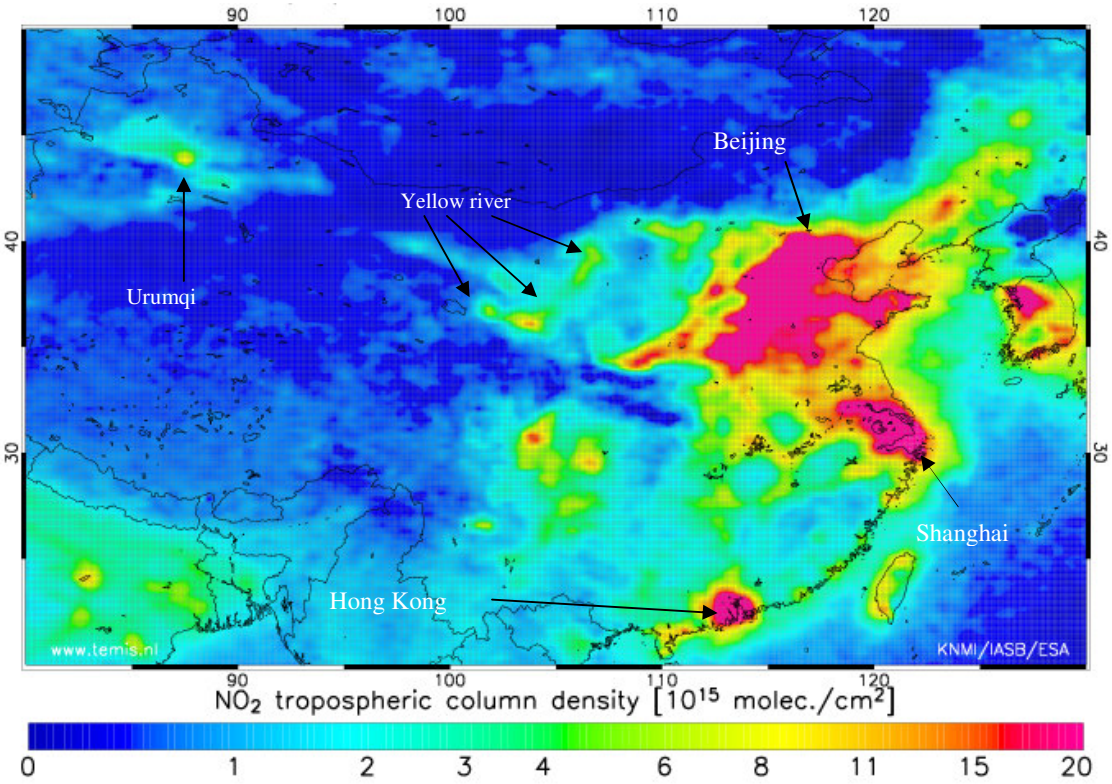

Figure 4.2. The yearly averaged tropospheric NO_2 column measured by SCIAMACHY for 2004.

4.3 Data analysis

The GOME data from March 1996 till March 2003 and the SCIAMACHY data from April 2003 till December 2004 have been used to analyze the trends and variability in NO_2 over China. April 2003 is the first month where SCIAMACHY NO_2 columns successfully are retrieved. The retrieved tropospheric NO_2 columns are gridded on a 1° by 1° grid, using weighting factors for the overlap between satellite pixel and grid cell, more information is given in appendix A. For each cell two time series are determined; a time series based on a two weeks average and one based on a monthly average. Both time series are tested for the best fit. Because of the larger sample the monthly average lead to a better and more consistent time series. The negligible weekly cycle of the NO_2 concentration above China makes it unnecessary to compensate for lower weekend measurements.
The temporal variability in the NO_2 columns is usually larger than the precision of the measurements. To account for both effects, the uncertainty of the monthly mean is determined by taking the sample standard deviation of the mean (see appendix A). The measurement error on the tropospheric NO_2 for individual pixels as calculated by [Boersma et al.,2004] shows a dependency on the absolute value of tropospheric NO_2, having a minimum error of about $1 \cdot 10^{15}$ molec/cm^2. This minimum error is used as lower limit for the error on the monthly average NO_2 concentration to avoid a non-realistic accuracy caused by a limited number of samples. In Figure 4.3 an example of a time series is given. The monthly average tropospheric NO_2 vertical column density is plotted against the number of months after January 1996. The small crosses are the monthly averaged values measured by GOME and SCIAMACHY. The solid line is the model fit and the remainder between model and measurement is denoted by the squares.

Two models have been used to fit the time series, a model with a linear trend and a seasonal component for the annual cycle of NO_2, and a model with an exponential trend. The model with the linear trend is described by the following function based on Wheaterhead et al. [1998],

$$Y_t = A + BX_t + C\sin(DX_t + E) + \delta U_t + N_t, \qquad (4.1)$$

where Y_t represents the monthly NO_2 column of month t and X_t is the number of months after January 1996, N_t is the remainder (residual unexplained by the fit function) and A,B,C,D,E,δ are the fit parameters. Parameter A represents the NO_2 column in January 1996, and B is the monthly trend in NO_2. The seasonal component contains amplitude C, a frequency D and a phase shift E. The fit of the frequency D leads to an expected period of one year, therefore this fit parameter was fixed for the final analyses. The data has also been fitted with a linear model, without a seasonal component. The analyses of this fit showed that the seasonal component was an essential part of the model. A linear growth was used to fit the time series since there is no large distinction between a linear and an exponential growth of the tropospheric NO_2 column over China in the period 1996 to 2004, which can be seen in Figure 4.3.

The term δU in equation 4.1 is used to fit the bias between the measurements of GOME and SCIAMACHY, where δ is the value of the bias and U_t is,

$$U_t = \begin{cases} 0 & t < T_0 \\ 1 & t \geq T_0 \end{cases}. \qquad (4.2)$$

In this equation the time T_0 ($0 < T_0 < T$) is the moment when the time series switches from using GOME to using SCIAMACHY data, which in this case is April 2003. The total number of months is denoted by T. The bias δ is fitted and checked for latitude dependence over China, We find that the bias is negligible, with values less than 0.01 10^{15} molec/cm^2. Based on this result the bias term is set to zero in analysis below.

The remainder, N_t in equation 4.1 is the difference between the model and the measured value. Weatherhead et al. [1998] suggest modeling the remainder by

$$N_t = \phi N_{t-1} + \varepsilon_t, \qquad (4.3)$$

where ε_t is the white noise and ϕ is the autocorrelation in the remainder. The autocorrelation in the remainder is a result from processes which are persistent with time and which are not described by the fit function, see Tiao et al. [1990]. We produced plots of the correlation between remainders as a function of the time difference. A typical autocorrelation of 0.1 is found, indicating that the remainders are only weakly correlated. The autocorrelation in the remainder affects the precision of the trend. In Wheaterhead et al. [1998] a derivation is given for the precision of the trend as function of the autocorrelation, the length T of the dataset in months and the variance in the remainder, σ_N (see appendix B).

The length of the dataset in years, n, is introduced to express the precision of the trend per year. For small autocorrelations the standard deviation σ_B of the trend per year is approximately given by

$$\sigma_B \approx \left[\frac{\sigma_N}{n^{3/2}} \sqrt{\frac{1+\phi}{1-\phi}} \right]. \qquad (4.4)$$

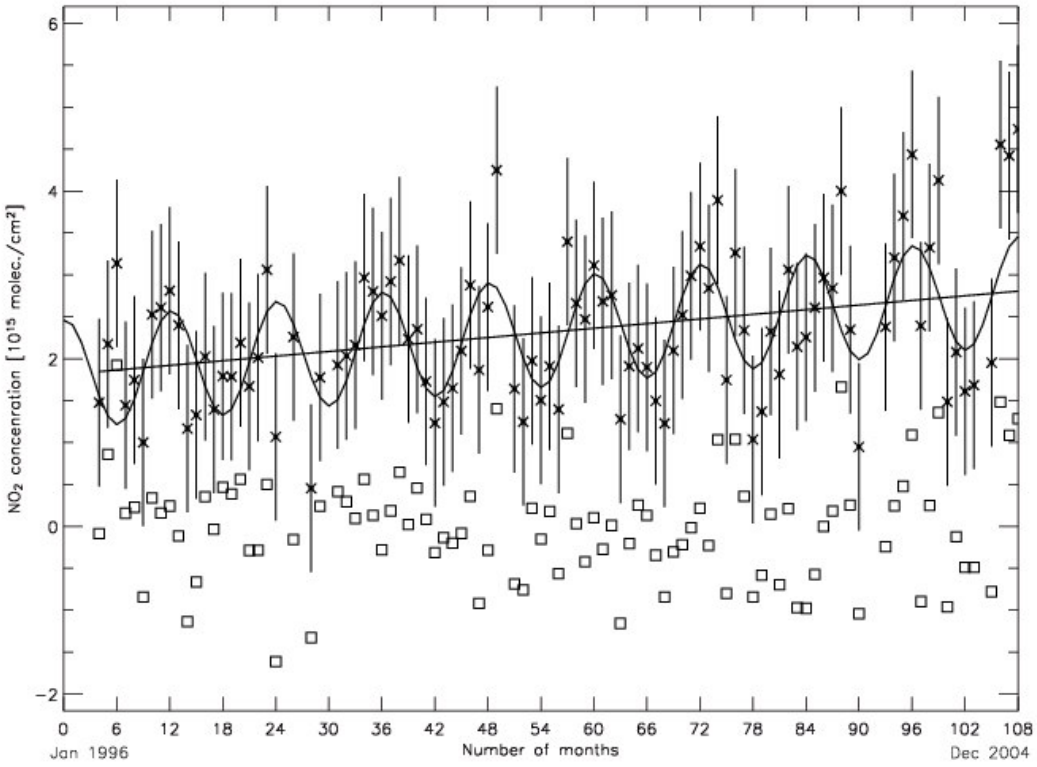

Figure 4.3. An example of a time series for one grid cell near Ji'an (115.5, 27.5). The Y-axis shows the monthly mean NO_2 tropospheric column and the X-axis shows the month index starting January 1996. The crosses mark the measurements by GOME and SCIAMACHY. The solid line is the fitting result, consisting of a linear growth and a seasonal component. The difference between fit and measurement is marked by the transparent squares.

4.4 Trend analysis

For each grid cell in China the model following equation 1, is applied, leading to a spatial distribution of each of the fitting parameters of the model. In Figure 4.4 the trend in NO_2 concentration is, shown as the yearly increase in tropospheric NO_2. In Figure 4.4 it can be seen that the trend is the highest in the eastern part of China. These regions with the highest trend correspond to the regions with a fast industrial and economical development. The fastest growing economy is in the Shanghai region, which also shows the largest growth of tropospheric NO_2. It is interesting to note that the growth in the region around Hong Kong is less than for other regions with a high economical activity. This is probably due to the already high level of economic activity in 1996 when our trend study started and a package of measures against air pollution in Hong Kong taken over the last years.

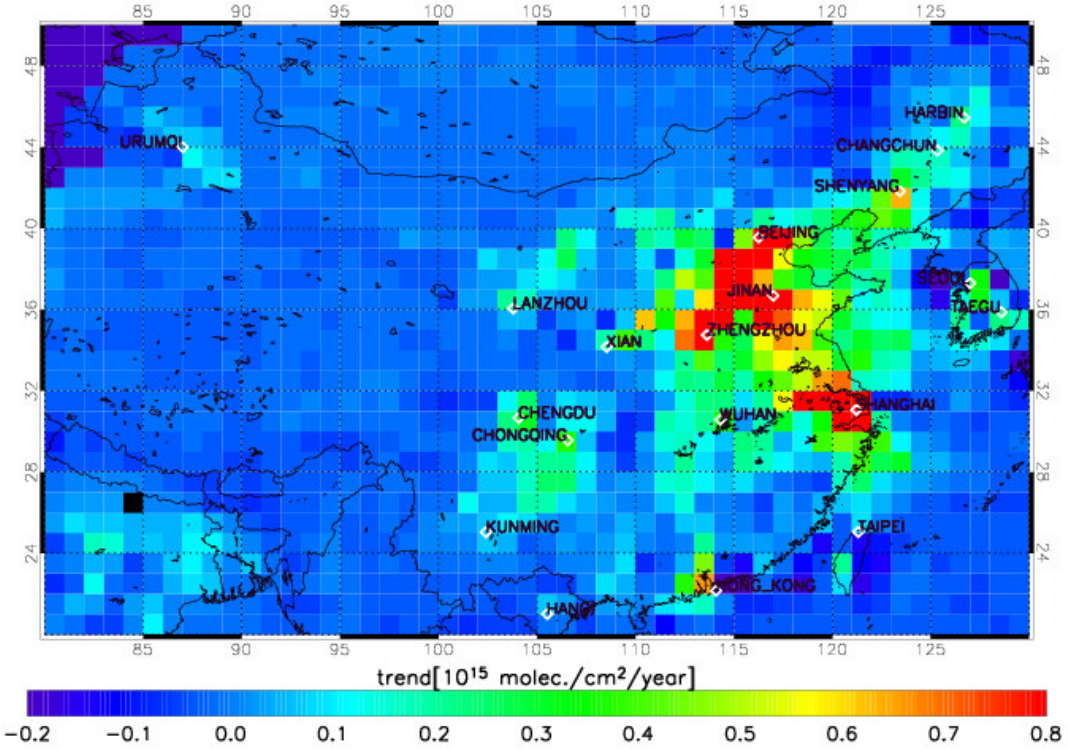

Figure 4.4. The trend of the NO_2 concentration over China for the period 1996-2004.

The precision σ_B of the trend on NO_2 is calculated using equation 4.4. In Figure 4.5 the trend divided by the precision is shown. It is a common decision rule for trend detection that a trend B is real with a 95% confidence level if $|B/\sigma_B| > 2$. Figure 4.5 shows that a significant trend (white grid cells) is detected in the regions of East China with a high population and high industrial activity. From equation 4 can be seen that the standard deviation of the trend decreases if the length of the dataset increases. Therefore, it can be expected that for more grid cells a significant trend can be detected with a longer dataset.

In Table 4.1 the trend estimates and start values for some major cities are shown. A yearly growth is determined in terms of percentage with respect to the start value in 1996. Shanghai is one of the fastest growing industrial areas, which is reflected in a large growth in NO_2. The trend over Taipei is not significant in this period. This is probably due to the effect of measures by the government to improve the air quality in Taiwan (see Taiwanese Environmental Protection Administration: *www.epa.gov.tw*).

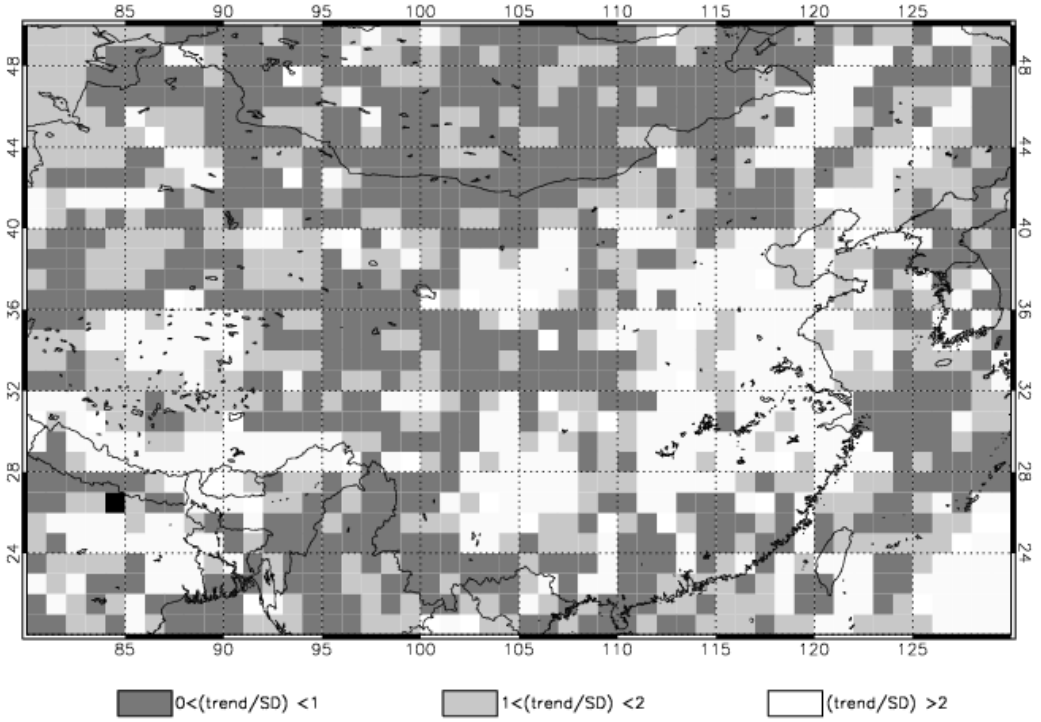

Figure 4.5. The NO_2 trend per year divided by the standard deviation. If this value is higher than 2 (white areas) a real trend is indicated with a 95% confidence level.

The increase of industrial and economical activity results in an increase of various types of emissions. For instance, an increase of aerosols may lead to higher sensitivity of the satellite measurements for NO_2 present within and above the aerosol layers. Therefore, it is possible that a measured trend in NO_2 concentration is enhanced by a trend in aerosols. However, Boersma et al. [2004] showed that satellite-derived cloud fractions are also sensitive to aerosols with a high single scattering albedo. An increase in retrieved cloud fractions over China could therefore be caused by an increase in scattering aerosols. A trend study of FRESCO monthly mean cloud fractions for situations with cloud fractions < 0.2 showed no significant increase in cloud fraction nor an appreciable decrease in the number of available observations. This suggests that the effect of aerosol changes in time on the derived trends in NO_2 may be neglected .

The tropospheric slant column is calculated by subtracting the stratospheric slant column from the total slant column. To derive the vertical tropospheric column the tropospheric slant column is divided by the tropospheric air mass factor. An additional trend study is performed on the stratospheric column and the tropospheric air mass factor to make sure that the observed trend originates from the tropospheric column. In Figure 4.6 the time series are shown for the vertical stratospheric column, the tropospheric air mass factor and the tropospheric column. The time series are based on the monthly averages for East China (110°-120°E, 20°-40° N). The tropospheric air mass factor is divided by the geometrical air mass factor to compensate for the viewing geometry effects. In the Figure it can be seen that there is a decreasing trend in the stratospheric column but this trend is not significant. However, the

tropospheric air mass factor shows a significant negative trend. This trend may be caused by changes in meteorological aspects like the temperature, boundary layer mixing, or cloud properties. To investigate the relation of the air mass factor trend and the observed trend in the tropospheric column, the spatial correlation is calculated between the relative yearly change in the air mass factor and the relative yearly change in the tropospheric column for all grid cells in East China. A small negative correlation of -0.14 is found for the geographical pattern of both trends. From this we conclude that there is not only a trend in tropospheric NO_2 but also changes in meteorological aspects. The small spatial correlation between the changes in the meteorological aspects and the trend in the NO_2 column led us conclude that the trend in the air mass factor is not the main raison for the trend in tropospheric NO_2.

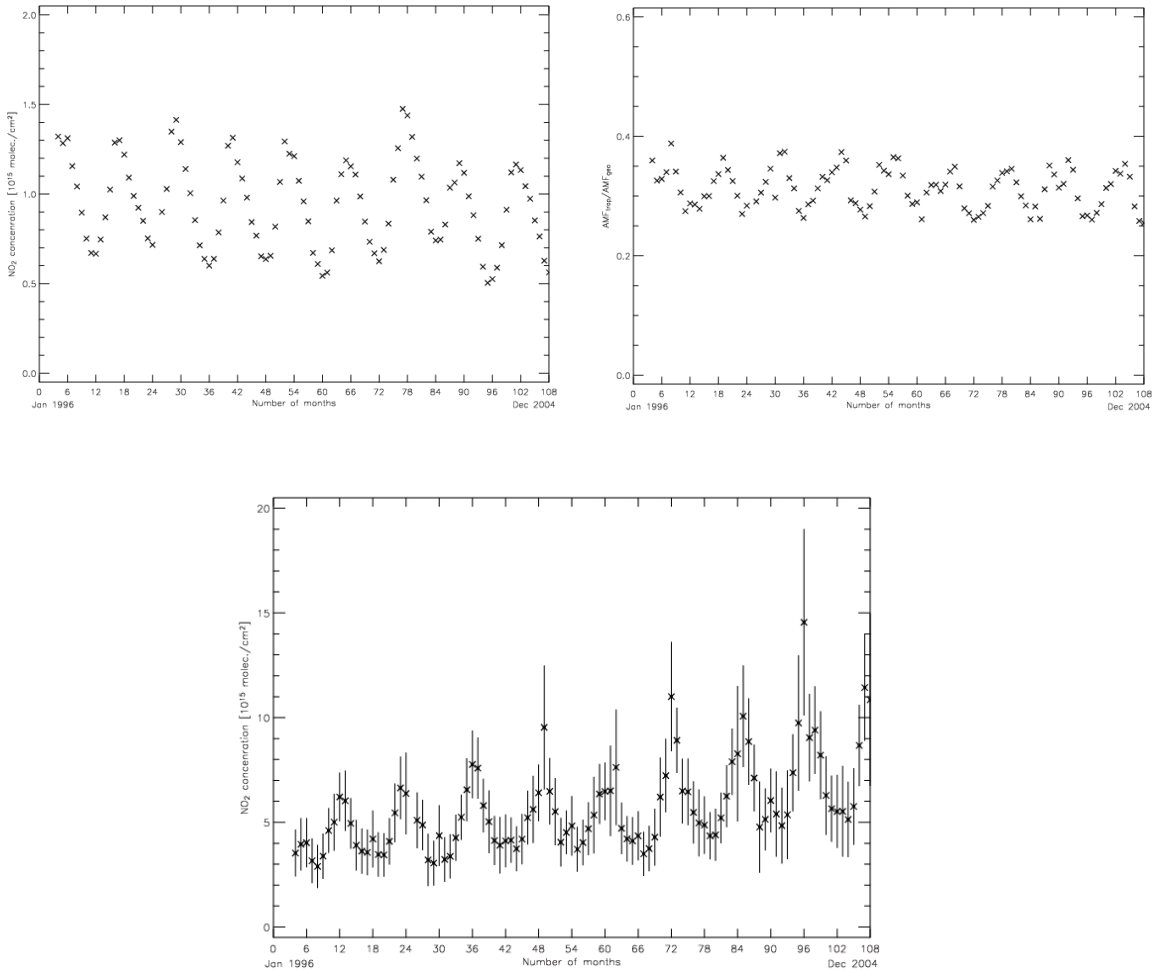

Figure 4.6. The time series of monthly averages of the tropospheric vertical column (bottom), the stratospheric vertical column (top left) and the tropospheric air mass factor divided by the geometrical air mass factor(top right). The monthly averages are calculated for East China (110°-120°E, 20°-40° N).

Table 4.1. The observed trends for some cities in East Asia. The percentage is calculated with respect to the year 1996.

	NO_2 concentration in January 1996 [10^{15} molec/cm^2]	Linear trend in NO_2 [10^{15} molec/cm^2/ year]	Error on trend [10^{15} molec/cm^2/year]	Growth (reference year 1996)
Hong Kong	7.63	0.72	0.48	8%
Beijing	10.92	1.20	0.48	11%
Shanghai	5.48	1.44	0.35	25%
Taipei	4.89	-0.02	0.06	0%
Chongqing	3.10	0.40	0.10	13%
Seoul	9.95	0.36	0.21	4%
Background 86°E x 40°N	0.5	0	0.01	0%

4.5 The NO_2 seasonal cycle

Equation 4.1 is used to study the seasonal cycle of the NO_2 concentration. Since the lifetime of NO_x is longer in the winter and emissions are higher, a NO_2 maximum is expected in the winter [Beirle et al., 2003]. Figure 4.7 shows that the month with the largest NO_2 abundances in the East and South of China is according to the expected winter maximum, but in the West a NO_2 maximum during summertime is found. The black grid cells correspond to regions where a linear fit works just as well but without a clear seasonal cycle.

The time series in Figure 4.6 illustrates the winter maximum in East China. For West China the time series of the tropospheric vertical column, the stratospheric vertical column and the tropospheric air mass factor are shown in Figure 4.8. In the Figure it can be seen that the variation in de modeled air mass factor is small with respect to variations in the tropospheric NO_2 column. The Figure shows that there is a summer maximum in the stratospheric column as well. However, the maximum error on the tropospheric column caused by errors in the stratospheric column is 0.35 10^{15} molec/cm^2 for West China. Therefore, we conclude that the air mass factor and the stratospheric NO_2 column are not the main reasons for the measured seasonal cycle of the tropospheric NO_2 column in West China.

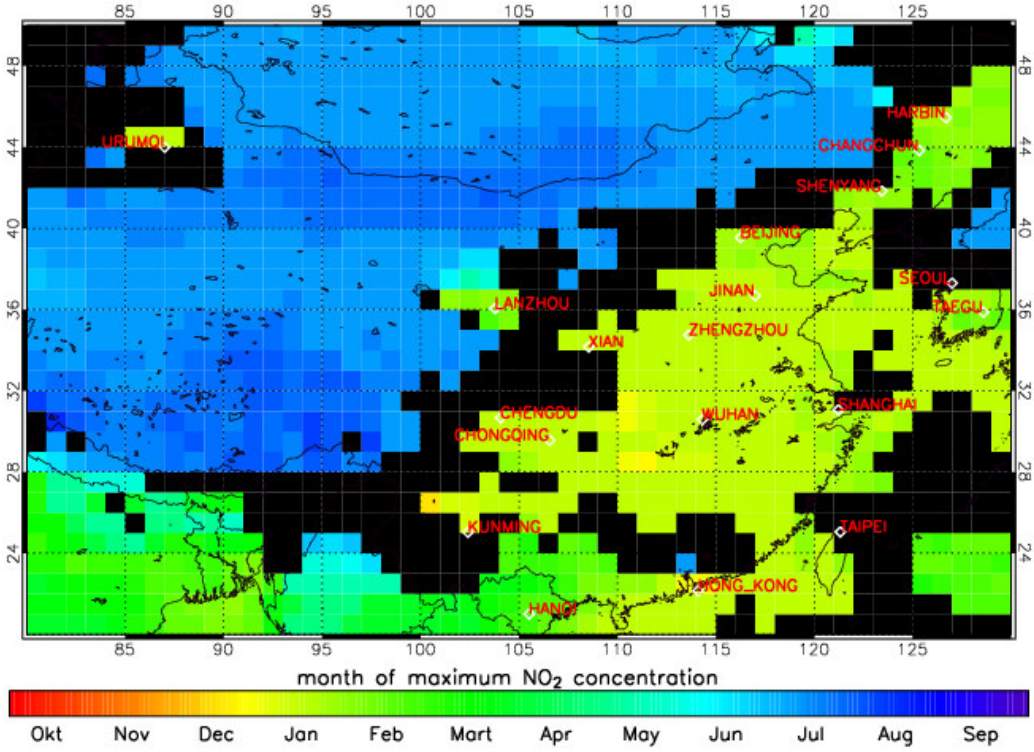

Figure 4.7. Map of China showing the month where the yearly seasonal component has its maximum in NO_2 concentration. In East China a maximum is found during the winter and in the West of China a maximum is found during the summer. The black pixels are regions where a linear fit without a seasonal component is more accurate.

The western part of China has a low population density (see Figure 4.1). As a consequence natural emissions are expected to dominate the tropospheric column. Figure 4.6 shows that in the North West, above the large city Urumqi, a winter maximum is found, which strengthens the idea that the summer maximum in NO_2 over the rest of West China is caused by natural emissions.

Lightning flash densities are measured by the Optical Transient Detector (OTD)(http://thunder.msfc.nasa.gov/OTDsummaries). From a comparison between the summer and winter flash densities can be concluded that lightning above China especially occurs during summertime. The contribution of lightning to the tropospheric NO_2 column is strongest in the tropics, with an estimated maximum of 0.4 10^{15} molec/cm^2 [Edwards et al., 2003, Boersma et al., 2005]. Because the difference between summer and winter tropospheric columns is typical of the order 1.0 10^{15} molec/cm^2, lightning alone cannot account for all the natural emissions in West China. Bryan et al. [2003] show that there is no biomass burning in the western part of China. In Yienger et al. [1995] it is suggested that in remote agriculture regions soil emissions contribute 50% to the total NO_x budget and that in July these percentages can rise to more than 75%. Yienger et al. [1995] also suggested that soil NO_x emissions are temperature dependent, soil dependent and precipitation dependent. A higher surface temperature leads to more NO_x emissions, which would explain higher NO_x

concentrations in summer time. They also found higher NO_x emissions for grassland that together with desert and scrub land form the main soil composition in West China. Another effect that increases soil NO_x emissions in summertime is "pulsing", which is described in [Yienger et al., 1995] and [Jaeglé et al., 2004] as an increase in NO_x measured after a shower of rain. From the IRI/LDEO Climate Data library it can be seen that in the West part of China it is only raining in the summer season. This also contributes to enhanced NO_2 concentrations during summertime. In appendix C more information is given on lightning and soil emissions over China.

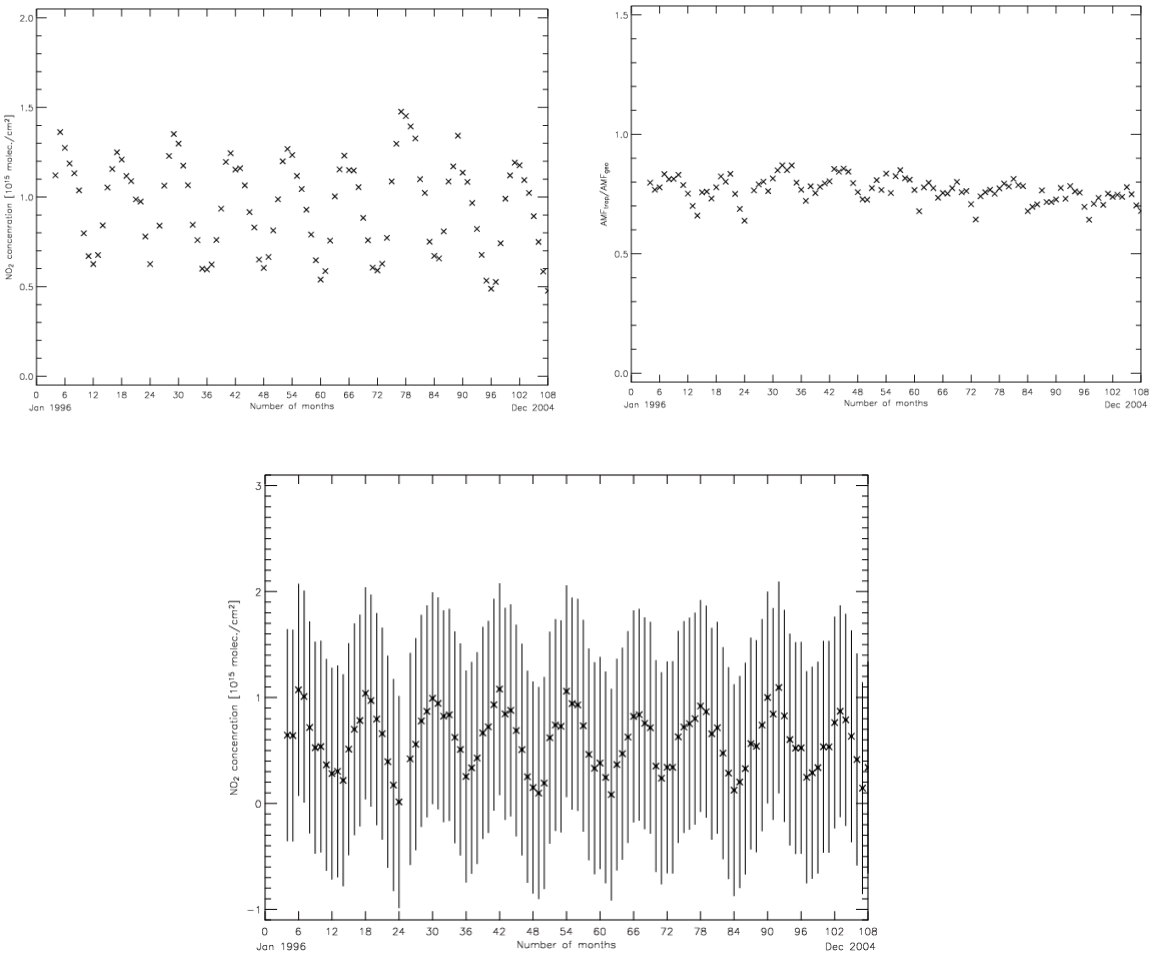

Figure 4.8. The time series of monthly averages of the tropospheric vertical column (down), the stratospheric vertical column (top left) and the tropospheric air mass factor divided by the geometrical air mass factor(top right). The monthly averages are calculated for West China (80°-100°E, 30°-42° N).

4.6 Conclusions

The tropospheric NO_2 columns measured by GOME and SCIAMACHY have been used for trend analysis over China. A linear model with a seasonal component is used to fit the time series of NO_2 concentrations. By applying this model to each grid cell a spatial distribution of the fit parameters is calculated. Furthermore the precision of the trend is calculated.

It can be concluded that the 9 years long NO_2 dataset from GOME and SCIAMACHY can be used for trend analysis in the eastern part of China. In this high populated and industrial area the trend is large enough to be significant. For instance Shanghai had a yearly increase of 25% in 1996. For other regions longer time series are needed to detect a significant signal.

The geographic distribution of the seasonal cycle of tropospheric NO_2 was studied. In the eastern part of China an expected winter maximum is found. In the western part of China this cycle shows a NO_2 maximum in summer time. As there is nearly no anthropogenic activity in Western China, this cycle is attributed to natural emissions, especially soil emissions and lightning.

The bias between the monthly GOME and SCIAMACHY tropospheric NO_2 series appears to be negligible and does not show any latitude dependence. This shows the consistency in the retrieval method of tropospheric NO_2 and allows the use of long time series by combining different instruments to detect a significant trend for regions without a large trend.

It is well known that emissions are increasing over China [Streets et al., 2003; Wang et al., 2004]; this study shows that the satellite measurements are able to measure the increase of atmospheric concentrations. New emissions inventories in combination with model studies are needed to decide whether the increase in the NO_2 column is fully caused by the increase of NO_x emissions or by changes in chemical regime.

5 Conclusions and Outlook

This study is an example of using satellite data for monitoring changes in the atmospheric composition. The satellite instruments GOME and SCIAMACHY provide a global dataset of tropospheric NO_2 of the last 10 years. This data is used to find answers on three questions on the tropospheric NO_2 column over China; 1) is there a trend and what is the value, 2) what is the seasonal cycle, and 3) how to interpret the answers to these questions.

We can conclude that the unique dataset is suitable for trend detection in tropospheric NO_2. In East China, above the economical developing regions, a significant trend is measured. The largest trend is found above Shanghai, with a yearly increase of 25% in the tropospheric NO_2. Other regions where a significant trend is detected include Beijing, Jinan, Chengdu and Chongqing.

The seasonal cycle of tropospheric NO_2 over China shows a difference between East and West China, this corresponds with the geographical distribution of the population density. A winter maximum is found for eastern China, where anthropogenic emissions dominate. In West China a summer maximum is found in the tropospheric NO_2 columns. This region is characterized by the dominance of soil emissions and lightning.

We concluded that the Chinese regions with an increase in NO_2 columns correspond with highly economical developing areas. However, there are worldwide more regions with comparable human activity. Therefore, it is interesting to do a global trend study to focus on regions like Western Europe and the United States, which are characterized by comparable emissions.

This study illustrates that from a 9 years dataset only a significant trend can be measured above the industrial hot spots. For other regions a longer dataset is required, to which can be contributed by the ozone monitoring instrument (OMI) aboard the recently launched platform EOS-AURA. The advantage of OMI is that it is able to produce daily global maps on a higher resolution.

The measured seasonal cycle gives an indication of the regional dominating NO_x source. By performing a global study on the NO_2 seasonal cycle it is possible to distinguish NO_x sources. For instance it is expected that satellites instruments can measure the seasonal variation of biomass burning over Africa.

The increased NO_x columns are caused by increasing emissions. However, it is difficult to translate a trend in the columns to a trend in emissions, because chemical regimes can be changed. For this translation chemical transport model runs are necessary: by comparing the measured columns with the model columns the emission database can be updated.
Chemical transport model runs are also necessary to distinguish the NO_x sources in West China, to quantify NO_2 from each of the sources, e.g. lightning or soil emissions.

6 References

Beirle, S., U. Platt,M. Wenig, and T. Wagner (2003), Weekly cycle of NO_2 by GOME measurements: a signature of anthropogenic sources, *Atmos Chem. Phys*., *3*, 2225 –2232

Blond, N., K.F. Boersma, H.J. Eskes, R.J. van der A, M. Van Roozendael, I. De Smedt, G. Bergametti, and R. Vautard (2005), Intercomparison of SCIAMACHY nitrogen dioxide observations, in-situ measurements, and air quality modeling results over Western Europe, submitted to *J. Geophys. Res*

Boersma, K.F., H.J. Eskes and E.J. Brinksma (2004), Error analysis for tropospheric NO2 retrieval from space, *J. Geophys. Res.*, *109*(D0) ,4311, doi: 10.1029/2003JD003961.

Boersma, K.F., H.J. Eskes, E.W. Meijer, and H.M. Kelder (2005), Estimates of lightning NO_x production from GOME satellite observations, *Atmos. Chem. Phys. Discuss.* 5, 3047-3104 (2005).

Boersma, K.F.(2005), Satellite observations of tropospheric nitrogen dioxide; retrieval interpretation and modelling*,* Ph.D Thesis, Universiteitsdrukkerij Technische Universiteit Eindhoven, Eindhoven

Brasseur, G.P., J.J. Orlando, (1999), *Atmospheric chemistry and Global changes*, Oxford University Press, Oxford

Bylin, G., (1993), Controlled studies on humans, Scand. J. Work Environ. Health. 19 , suppl 2, pp 37-43

Bryan N. D., R.V. Martin, A.C. Staaudt, R.Yevich, and J.A. Logan. (2003),Interannual and seasonal variability of biomass burning emissions constrained by satellite observations, J. *Geophys. Res*., *108* (D2), 4100, doi:10.1029/2002/JD002378

Dentener, F.,M. van Weele, M. Krol, S Houweling, and P. van Velthoven (2003), Trends and inter-annual variability of methane emissions derived from 1979-1993 global ctm simulations, *Atmos. Chem. Phys., 3,* 73-88

Edwards, D. P., J.F. Lamarque, J.L, Attie, L. K. Emmons, A. Richter, J.P. Cammas, J. C. Gille, G. L. Francis, M. N. Deeter, J. Warner, D. C. Ziskin, L. V. Lyjak, J. R. Drummond, and J. P. Burrows (2003), Tropospheric Ozone Over the Tropical Atlantic: A Satellite Perspective, *J. Geophys. Res*, *108*(D8), 4237, doi:10.1029/2002JD002927,

Eskes, H. and F. Boersma (2003), Averaging Kernels for DOAS total-column satellite retrievals. *Atmos Chem. Phys*., *3*, 1285 – 1291, 2003

European Commission. Working group on Nitrogen Dioxide, (1997), Position paper on Air Quality: nitrogen dioxide, http://europa.eu.int/comm/environment/air/pdf/pp_no2.pdf

Fayt, C., Van Roozendael, M.:WinDOAS 2.1 Software User Manual, 2001, http://www.oma.be/GOME/GOMEBrO/WinDOAS-SUM-210b.pdf.

Jacob, D.J.(1999), *Introduction to atmospheric chemistry*, Princeton University Press, Princeton

Jaeglé, L., R.V.Martin, K.Chance, L.Steinberger, T.P. Kurosu, D.J. Jacob, A.I.Modi, V.Yoboué, L. Sigha-Nkamdjou, and C.Galy-lacaux (2004), Satellite mapping of rain-induced nitric oxide emissions from soils, *J. Geophysical. Res* ,*109*(D2), 1310, doi:10.1029/2004JD004787

Kleinman, L.I., (1994), Low and high NO_x tropospheric photochemistry, *J. Geophys. Res*., *99*, 16.831-16.838

Koelemeijer, R.B.A., J.F. de Haan, and P. Stammes (2003), A database of spectral surface reflectivity in the range 335-772 nm derived drom 5.5 years of GOME observations, *J. Geophys. Res.,108*(D2), doi: 10.1029/2002JD002429

Leue, C., M. Wenig, T. Wagner, O. Klimm, U. Platt, and B. Jähne (2001), Quantitative analysis of NO_x emissions from Global Ozone Moinitoring Experiment satellite image sequences, *J. Geophys. Res,106*, 5493-5505

Martin, R.V., K.V. Chance, D.J.Jacob, D.J., Kursou, T.P., Spurr, R.J.D., Bucsela, E., Gleason, J.F., Palmer, P.I., Bey, I., Fiori., A.M., Li, Q. and Koelemeijer, R.B.A.(2002), *An improved retrieval of tropospheric nitrogen dioxide from GOME, J. Geophys. Res,107*(D20)4437*,* doi:10.10129/2001JD001027

Martin, R.V., D.J. Jacob, K.V. Chance, T.P. Kurosu, P.I. Palmer, and M.J. Evans (2003), Global inventory of Nitrogen Dioxide Emissions Constrained by Space-based Observations of NO_2 Columns, *J. Geophys. Res., 108*(D17), 4537, doi:10.1029/2003/JD003453

National Bureau of Statistics (NBS) (2004), *China Statistical Year Book 2003*, China statistics press, Beijing

Olivié, D.J.L.(2005), On the role of convection and turbulence for tropospheric ozone and its precursors*,* Ph.D Thesis, Universiteitsdrukkerij Technische Universiteit Eindhoven, Eindhoven

Olivier, J.G.J. , A.F. Bouwman, Van Der Hoek, K.W. and J.J.M. Berdowski (1998), Global Air Emission Inventories for Anthropogenic Sources of NOx, NH3 and N2O in 1990, *Env. Poll*., *102*, 135-148

Parton, W.J., E.A. Holland, S.J. Del Grosso, M.D. Hartman, R.E. Martin, A.R. Mosier, D.S. Ojima, and D.S. Schimel (2001), Generalized model for NO_x and N_2O emissions from soils, *J. Geophys. Res., 106*(D15), doi: 10.1029/2001JD900101

Platt, U.(1994), Differential Optical Absorption Spectroscopy (DOAS), in *Air Monitoring by Spectroscopic Techniques, Chem. Anal., vol. 127, edited by M.W. Sigrist, pp. 27-76, Wiley-Interscience, Hoboken, N.J.*

Richter, A., and J. P. Burrows, Tropospheric NO_2 from GOME measurements, *Adv. Space Res., 29,* 1673-1683 (2002).

Sierk, B., A. Richter, A. Rozanov, Ch. von Savigny, A.M. Schmoltner, M. Buchwitz, H. Bovensmann, and J.P. Burrows, (2004), Retrieval and Monitoring of atmospheric trace gas concentrations in nadir and limb geometry using the space-borne SCIAMACHY instrument, presented at the "5th International Symposium on Advanced Environmental Monitoring", submitted to "*Environmental Monitoring and Assessment*"

Streets, D.G., T.C. Bond, G.R. Carmichael, S.D. Fernandes, Q. Fu, D. He, Z. Klimont, S.M. Nelson, N.Y. Tsai, M.Q. Wang, J.-H. Woo, and K.F. Yarber (2003), An inventory of gaseous and primary aerosol emissions in Asia in the year 2000 *J. Geophys. Res., 108*(D21), 8809, doi:10.1029/2002JD003093

Tiao, G.C. Reinsel, Daming XU, J.H. Pedrick, Xiaodong Zhu, A.J. Miller, J.J. DeLuisu, C.L. Mateer, and D.J. Wuebbles (1990), Effects of autocorrelation and temporal sampling schemes on estimates of trend and spatial correlation, *J. Geophys. Res.*, *95*,20.507-20.517

Wang, Y. X., and M.B. McElroy (2004), Asian emissions of CO and NO_x: Constraints from aircraft and Chinese station data, *J. Geophys. Res*, *109*,(D2),4304, doi:10.1029/2004JD005250.

Weatherhead, E.C., G.C. Reinsel, G.C. Tiao, X. Meng, D. Choi, W. Cheang, T. Keller, J. DeLuisi, D. J. Wuebbles, J.B. Kerr, A.J. Miller, S. J. Oltmans, and J.E. Frederick (1998), Factors affecting the detection of trends: Statistical considerations and applications to environmental data, *J. Geophys. Res*., *103*, 17.149-17.161

Yaffee, R.A., M. Mc Gee (2000), *Introduction to time series analysis and forecasting: with applications of SAS and SPSS*, Academic Press, London

Yienger J.J., and H. Levy II(1995), Empirical model of global soil-biogenic NO_x emissions, *J. Geophys. Res.*, *100*, 11.447-11.464

7 Acknowledgements

I would like to give special thanks to Ronald van der A, my supervisor at the KNMI. I am Ronald very thankful for the comments, input and discussion on my research study, he let me enjoy science. I also need to thank Ronald and Hennie Kelder for arranging funding for my trip to Beijing and two conferences, which I enjoyed very much. A grateful word I have to address to Hennie Kelder, for awaking my interest on atmospheric physics and giving me this opportunity to do this study.
There are many other people from the Atmospheric Composition division of the KNMI who helped me during this year. I will not name them all, except Folkert Boersma, I would thank him for having always time for discussion. Because I had RSI symptoms, after my visit of Beijing, I also want to thank my brother and mother for helping me with writing this report.

Appendix A. Data analysis

GOME has a pixel size of 320 km by 40 km and SCIAMACHY has a pixel size of 60 km by 30 km. To do trend study the satellite measurements are redistributed to a fixed grid. In this research a grid with a 1° by 1° resolution is chosen. This choice is based on the finest possible grid without loosing the representativity of the satellite measurement and having enough number of measurements for each grid cell.

The satellite measured pixels are gridded by using weighting factors for the overlap between the satellite pixel and the grid cell, see Figure A1 for an example. The weight factor (w_i) is the fraction of the satellite pixels that is covers a grid cell.

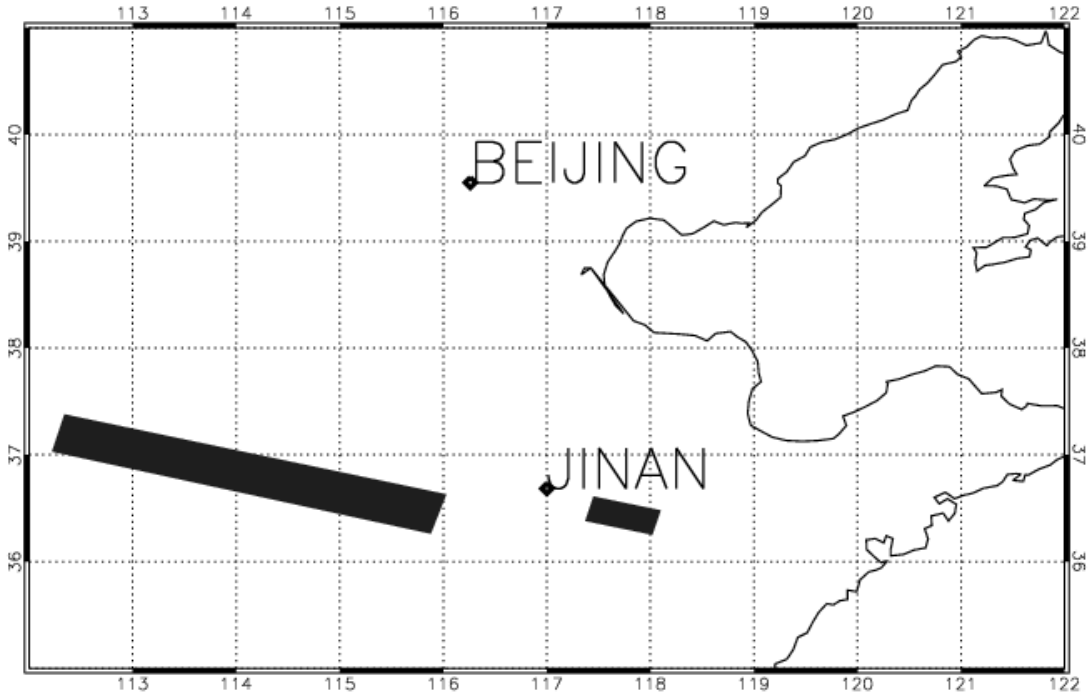

Figure A1. Example of a GOME satellite pixel (large) and a SCIAMACHY pixel (small) over a 1° by 1° grid.

The monthly average columns for one grid cell are calculated by taking the weighted average of all measurements in one month covering the grid cell,

$$\bar{y} = \frac{\sum_{i=1}^{L} w_i y_i}{\sum_{i=1}^{L} w_i}, \qquad \text{(A1)}$$

where y_i is the measured tropospheric NO_2 column and $\bar{y}$ is the best estimated monthly average NO_2 column based on the sample. L is the total number of measurements for one grid cell in one month. In this way time series based on monthly averages are made for each grid cell. Also time series based on a two weeks period are tested. But this leads to higher variability in the two weeks average columns due to small sample sizes and does not increase the significance of the fit parameters.

To fit time series realistic an error bar is needed for the monthly average column density. In Boersma et al. [2004] a quantitative error analysis is given for the tropospheric NO_2 column; therefore it is possible to calculate an error on the column density, based on the retrieval method. However, the variability in the NO_2 column during a month is usually higher than the precision of the measurements. Therefore the precision of the monthly mean is determined by taking the standard deviation of the mean (σ_m). Because we use weight factors for pixel overlap, the sample standard deviation (σ_{ssd}) is calculated by,

$$\sigma_{ssd}^2 = \frac{\sum_{i=1}^{L} w_i (y_i - \bar{y})^2}{\sum_{i=1}^{L} w_i}. \tag{A2}$$

To calculate the standard deviation of the mean, we introduce the monthly mean μ.

$$\sigma_{ssd}^2 = \frac{\sum_{i=1}^{L} w_i \left\{ (y_i - \mu) - (\bar{y} - \mu) \right\}^2}{\sum_{i=1}^{L} w_i} = \frac{\sum_{i=1}^{L} w_i (y_i - \mu)^2}{\sum_{i=1}^{L} w_i} + \frac{\sum_{i=1}^{L} w_i (\bar{y} - \mu)^2}{\sum_{i=1}^{L} w_i} - 2\frac{\sum_{i=1}^{L} w_i (y_i - \mu)(\bar{y} - \mu)}{\sum_{i=1}^{L} w_i}. \tag{A3}$$

The first term on the right hand side is the squared of the standard deviation (σ^2), the second term on the right hand side is the squared of the standard deviation of the mean (σ_m^2), the last term can be written as twice the squared of the standard deviation of the mean. Therefore, equation A3 can be written as,

$$\sigma_{ssd}^2 = \sigma^2 - \sigma_m^2. \tag{A4}$$

The relation between σ^2 and σ_m^2 can be determined from expression A1 and applying error propagation. Based on error propagation the standard deviation of the mean can be calculated from equation A1,

$$\sigma_m^2 = \sum_{i=1}^{L} \left(\frac{\partial \bar{y}}{\partial y_i} \sigma_{y_i}\right)^2 . \tag{A5}$$

From equation A1 can be derived that,

$$\frac{\partial \bar{y}}{\partial y_i} = \frac{w_i}{\sum_{i=1}^{L} w_i} . \tag{A6}$$

The standard deviation on a single measurement σ_{y_i} is taken constant σ for all measurements. We can write equation A5 now as,

$$\sigma_m^2 = \left(\frac{\sigma^2}{(\sum_{i=1}^{L} w_i)^2} \right) \sum_{i=1}^{L} w_i^2 . \tag{A7}$$

We now have a relation between combining σ^2 and σ_m^2. Combining equation A4 and A7 leads to the standard deviation of the mean for a sample,

$$\sigma_m^2 = \frac{\sigma_{ssd}^2}{\left\{ \frac{\left(\sum_{i=1}^{L} w_i \right)^2}{\left(\sum_{i=1}^{L} w_i^2 \right)} - 1 \right\}} . \tag{A8}$$

The measurement error on the tropospheric NO_2 column as calculated by Boersma et al. [2004] shows a dependence on the absolute value of the column. The error has a minimum of approximately $1 \cdot 10^{15}$ molec/cm^2, see Figure 2.4. This minimum error is caused by errors in the total slant column and the slant stratospheric column. The minimum error is used as lower limit for the error on the monthly average NO_2 concentration to avoid a non-realistic accuracy caused by a limited number of samples.

Appendix B. Precision of the trend

We will derive an approximation of the precision of the trend (σ_B) in equation 4.1. This precision is used to estimate whether the measured trend is significant. In this derivation the seasonal component and the intervention term are omitted. According to Wheaterhead et al. [1998] omitting the seasonal component does not have much influence on the statistical properties of the other fit parameters. However the seasonal component is essential for modeling the time series. To make this omitting plausible, the covariance matrix is calculated numeric for several pixels. From this covariance matrix the correlation matrix is obtained. This matrix shows that there is not a large correlation between the seasonal component and the trend.

The advantage of omitting the seasonal component is that we can derive an analytical expression for the precision of the trend. The number of months is denoted by *T*. The model is expressed in the form,

$$\mathbf{Y} = \mathbf{X}\boldsymbol{\beta} + \mathbf{N}, \tag{B1}$$

where **Y** is the *T x 1* vector of the monthly means and *T* is the number of months. **β** represents the fit parameters (*A,B*)' and **N** is the T x 1 vector of the noise terms. **X** is a T x 2 matrix and consists of a constant and a time series, expression B1 can also be written as

$$\begin{pmatrix} Y_1 \\ Y_2 \\ \vdots \\ Y_T \end{pmatrix} = \begin{pmatrix} 1 & 1 \\ 1 & 2 \\ 1 & \vdots \\ 1 & T \end{pmatrix} \cdot \begin{pmatrix} A \\ B \end{pmatrix} + \begin{pmatrix} N_1 \\ N_2 \\ \vdots \\ N_T \end{pmatrix}. \tag{B2}$$

The remainder **N** is the unexplained part, it is assumed that **N** is autoregressive of the first order,

$$N_t = \phi N_{t-1} + \varepsilon_t, \tag{B3}$$

where N_t is the remainder of month *t*, ϕ is the autocorrelation in the noise and ε_t are random and independent variables with mean zero, a variance of σ_ε^2 and $\mathrm{cov}(\varepsilon) = \sigma_\varepsilon^2 I$. It will be assumed that $-1 < \phi < 1$. Tiao et.al. [1990] showed that this model is adequate for taking account of autocorrelation, which frequently exist in atmospheric data. It follows that if equation B3 is written as $N_t - \phi N_{t-1} = \varepsilon_t$, the noise vector **N** can be transformed to **ε** by multiplication of matrix **P**. Matrix **P** can be expressed as

$$\mathbf{P} = \begin{pmatrix} \sqrt{1-\phi^2} & 0 & \cdots & \cdots & 0 \\ -\phi & 1 & 0 & \cdots & 0 \\ 0 & \ddots & \ddots & \ddots & \vdots \\ \vdots & \ddots & \ddots & \ddots & 0 \\ 0 & \cdots & 0 & -\phi & 1 \end{pmatrix}. \qquad \text{(B4)}$$

Taken the (1,1) element equal to $\sqrt{1-\phi^2}$ is suggested by Wheaterhead et al. [1998]. This is adopted from the Prais-Winsten algorithm to utilize the first observation [Yaffee, 2000]. The model for the time series of equation B1 will now be transformed by multiplying B1 with **P**,

$$\begin{aligned} \mathbf{PY} &= \mathbf{PX\beta} + \mathbf{PN} \\ \mathbf{Y}^* &= \mathbf{X}^*\boldsymbol{\beta} + \boldsymbol{\varepsilon} \end{aligned} \quad . \qquad \text{(B5)}$$

The advantage of this transformation is that the properties of the remainder $\boldsymbol{\varepsilon}$ allow us to apply the Ordinary Least Squares (OLS) method. The precision of the trend can be found in the covariance matrix of the OLS best estimate $\hat{\boldsymbol{\beta}} = \left(\mathbf{X}^{*\prime}\mathbf{X}^*\right)^{-1}\mathbf{X}^{*\prime}\mathbf{Y}^*$. $Cov\left(\hat{\boldsymbol{\beta}}\right)$ is given by

$$\begin{aligned} \operatorname{cov}\left(\hat{\boldsymbol{\beta}}\right) &= \operatorname{cov}\left\{\left(\mathbf{X}^{*\prime}\mathbf{X}^*\right)^{-1}\mathbf{X}^{*\prime}\mathbf{Y}^*, \mathbf{Y}^{*\prime}\mathbf{X}^*\left(\mathbf{X}^{*\prime}\mathbf{X}^*\right)^{-1}\right\} \\ &= \left(\mathbf{X}^{*\prime}\mathbf{X}^*\right)^{-1}\mathbf{X}^{*\prime}\operatorname{cov}\left\{\mathbf{Y}^*, \mathbf{Y}^{*\prime}\right\}\mathbf{X}^*\left(\mathbf{X}^{*\prime}\mathbf{X}^*\right)^{-1} \\ &= \sigma_\varepsilon^2\left(\mathbf{X}^{*\prime}\mathbf{X}^*\right)^{-1}, \end{aligned} \qquad \text{(B6)}$$

where $\mathbf{X}^{*\prime}\mathbf{X}^*$ is a 2 x 2 matrix,

$$\mathbf{X}^{*\prime}\mathbf{X}^* = \begin{pmatrix} h_1 & h_2 \\ h_2 & h_3 \end{pmatrix}. \qquad \text{(B7)}$$

The variance of the trend is given by the (2,2) element of the covariance matrix,

$$\operatorname{var}\left(\hat{B}\right) = \sigma_\varepsilon^2 \frac{h_1}{h_1 h_3 - h_2^2}, \qquad \text{(B8)}$$

The elements h_1,h_2 and h_3 will shortly be worked out.

$$h_1 = \sum_{u=1}^{T} X_{1u}^{*}\,'X_{u1}^{*} = \left[\sqrt{1-\phi^2},1-\phi,\ldots,1-\phi\right]\begin{bmatrix}\sqrt{1-\phi^2}\\1-\phi\\\vdots\\1-\phi\end{bmatrix} = (T-1)(1-\phi)^2+\left(1-\phi^2\right) \tag{B9}$$

$$\begin{aligned} h_2 = \sum_{u=1}^{T} X_{1u}^{*}\,'X_{u2}^{*} &= \left[\sqrt{1-\phi^2},1-\phi,\ldots,1-\phi\right]\begin{bmatrix}\sqrt{1-\phi^2}\\2-\phi\\\vdots\\T-(T-1)\phi\end{bmatrix} \\ &= (1-\phi)\left[\frac{T(T-1)}{2}(1-\phi)+\phi+T\right] \end{aligned} \tag{B10}$$

$$h_3 = \sum_{u=1}^{T} X_{2u}^{*}\,'X_{u2}^{*} = \left[\frac{1}{6}T(T+1)(2T+1)(1-\phi)^2+T^2\phi(1-\phi)+T\phi-\phi^2\right] \tag{B11}$$

To calculate h_3 the relation $\sum_{n=1}^{T} n^2 = \frac{1}{6}T(T+1)(2T+1)$ is used. The last two terms on the right hand side of B11 is the correction for using $n = u^2(1-\phi)^2$ in stead of $n = (u-(u-1)\phi)^2$. For small autocorrelations and large a T a close approximation for equation B8 is,

$$\mathrm{var}\left(\hat{B}\right) \approx \sigma_\varepsilon^2 \frac{12}{T^3(1-\phi)^2}. \tag{B12}$$

The relation between σ_ε^2 and σ_N^2 can be derived from expression B3,

$$\sigma_N^2 = \frac{\sigma_\varepsilon^2}{(1-\phi^2)}. \tag{B13}$$

With this relation the final approximation for the precision of the monthly trend (σ_{BM}) can be found by taking the square root of B12,

$$\sigma_{BM} \approx \frac{\sqrt{12}\sigma_N}{T^{3/2}}\sqrt{\frac{(1+\phi)}{(1-\phi)}}. \tag{B14}$$

In the article a trend per year is used (σ_B). For a precision on the trend per year equation B14 can be written as,

$$\sigma_B \approx \frac{\sigma_N}{n^{3/2}}\sqrt{\frac{(1+\phi)}{(1-\phi)}}, \tag{B15}$$

where *n* is the number of years.

Appendix C. Background on natural emissions.

In the introduction to NO_x chemistry is mentioned that soil emissions and lightning are the two main natural NO_x sources. In this appendix we will work out these two sources. It will be shown that the natural sources in West China lead to NO_2 columns with a summer maximum. Based on the vegetation type and the seasonal pattern of rain, temperature and lightning we conclude that soil emissions and lightning are the sources of the summer maximum.
First the main properties that effect the soil emissions are discussed. This is done by a small literature overview. Secondly, these properties are used to show that the NO_2 summer maximum is mainly caused by soil emissions. Third, it is shown that lightning over west China only occurs during summertime.

Soil emissions
NO_x emissions from soil are a result of microbial processes. The emissions are a by product of nitrification and denitrification [Parton et.al., 2001]. Nitrification is the conversion of NH_4 to NO_3 by bacteria and denitrification is the conversion of NO_3 to N_2. Parton et.al. [2001] used a model to calculate the N_2O soil emissions. Subsequently, they determined a NO_x: N_2O emission proportion based on soil parameters to calculate the NO_x emissions. They used input parameters like NH_4 and NO_3 concentrations, water filled pore space, temperature, PH, texture and rain events. Yienger et al. [1995] used a model to calculate direct the NO_x emissions based on temperature, vegetation type, precipitation, nitrogen fertilisation, soil moisture, biomass burning and canopy reduction.

The simulated NO_x emissions from both models show a seasonal pattern with a summer maximum. They also show a large contribution and influence of rain events on NO_x emissions. In Jaeglé et al. [2004] is shown that GOME is able to measure higher NO_x concentration after a shower of rain. According to Yienger et al. [1995] the strongest contribution to global soil emissions are agriculture, grassland and tropical rain forest.

We will now focus on China and the parameters, which are available for China. The relation between soil NO_x emissions and temperature, vegetation type and rain events is given for China. The soil temperature has a maximum in summer. This contributes to the expectation that the emissions have a maximum in summertime, because there is a positive correlation between soil temperature and soil NO_x emissions [Yienger et al., 1995]. The vegetation type is an other important parameter for describing soil emissions. In Figure C1 the vegetation of China is given. In the Figure, it can be seen that the main vegetation type in west China is grassland, scrubland and desert. According to Yienger et al. [1995] NO_x soil emissions can be expected in summertime for grassland and scrubland. The global model of Yienger et al. [1995] does not include the possibility that dessert and arid scrubland have NO_x emissions. However, they suggest that those areas might have emissions induced by rain also known as the “pulsing effect”.

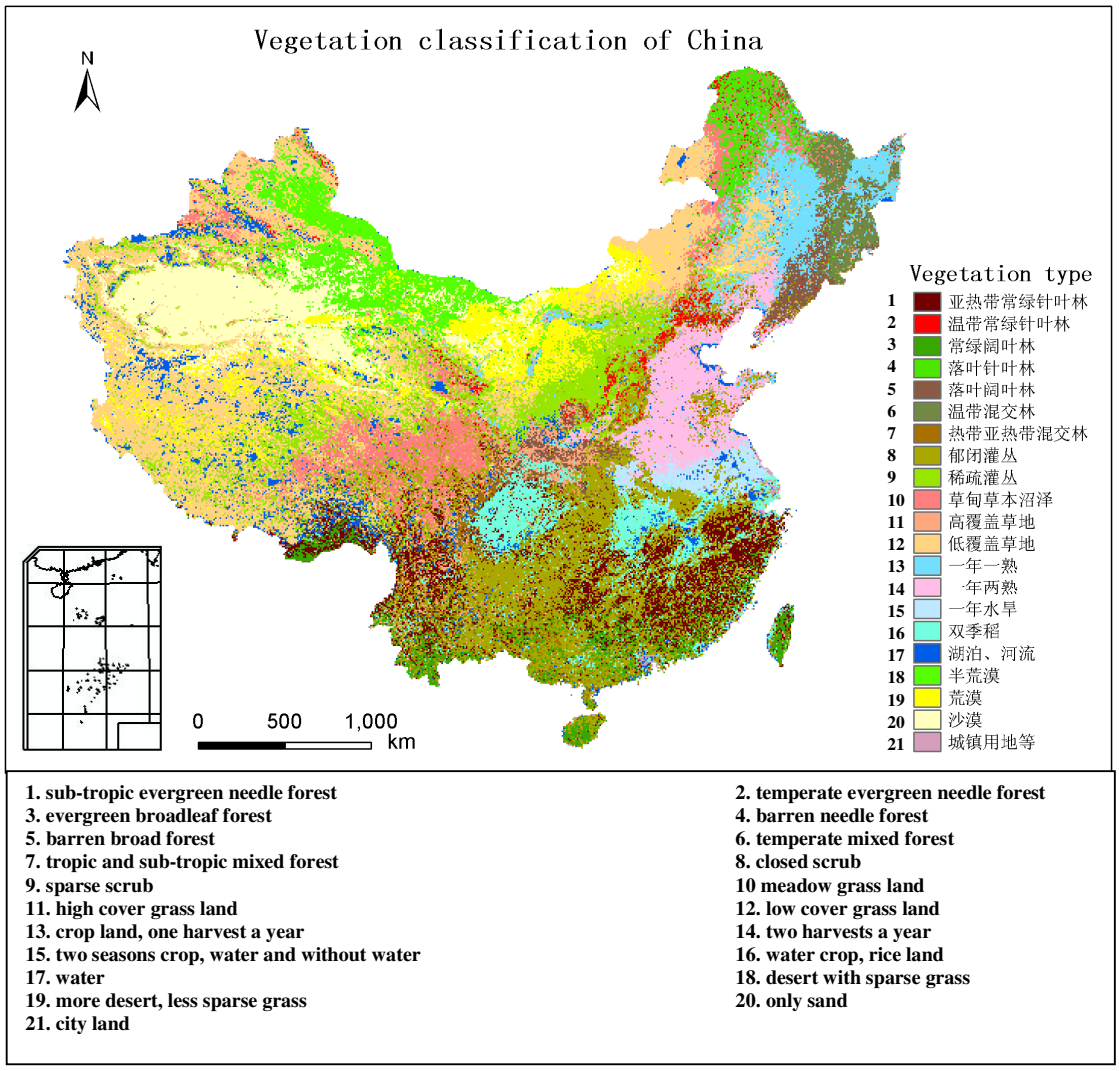

Figure C1. The vegetation type in China based on MODIS data. This plot is provided by Dr. Guicai Li from the NSMC in China.

The work of Yienger et al. [1995], Parton et al. [2001] and Jaeglé et al. [2004] show the importants of the pusling effect. Therefore, we will have a closer look on the rain data. In Figure C2 are examples shown of the average rain fall for some weather stations in West China. It can be seen that the rain fall in West China occurs mostly during summertime.

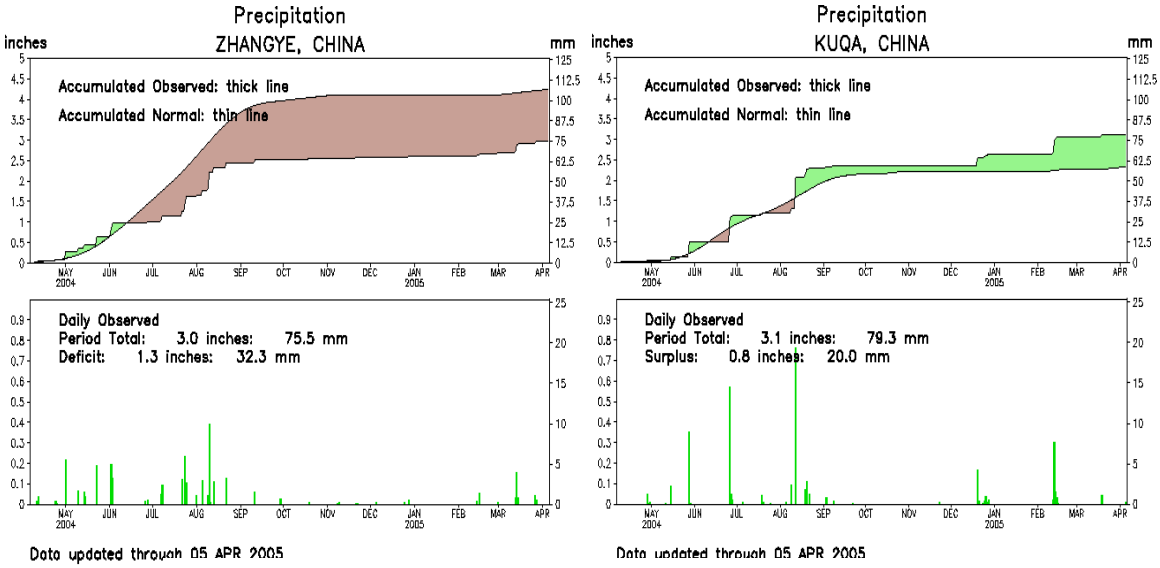

Figure C2. The yearly average accumulated rain (up) and the last year rain events (down) for Zhangye (38.9, 100.5) and Kuqa (41.7, 82.9) in West China. Time series for other weather stations can be found at the *Climate Prediction Centre (www.nws.noaa.gov).*

The result of these studies strengthens the idea that the measured summer maximum is partly caused by soil emissions.

Lightning

Rain showers often induce lightning, which creates NO_x. Figure C3 shows the number of lightning events in January 1998 and July 1998, observed by the Optical Transient Detector (OTD). In the Figure, it can be seen that lightning in West China only occurs during the summer. Here, we only show the numbers of lightning events for the year 1998, however, the other years show the same seasonal pattern. Data of the other years can be found at *http://thunder.msfc.nasa.gov/data/OTDsummaries/.*

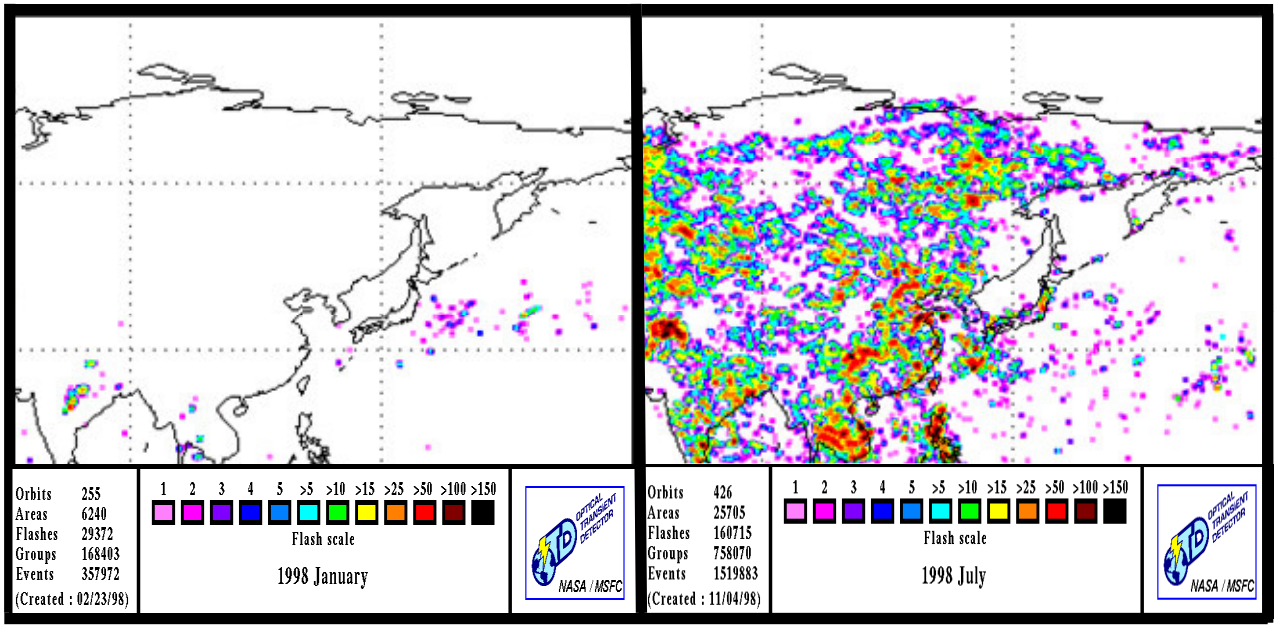

Figure C3. The number of lightning events in China for January (left) and July (right) 1998, from *http://thunder.msfc.nasa.gov/data/OTDsummaries/*